The Borris Field Experiment: Observations of Smoke Diffusion in the Surface Layer over Homogeneous Terrain

Mikkelsen, Torben

Publication date:
1983

Document Version
Publisher's PDF, also known as Version of record

Risø-R-479

THE BORRIS FIELD EXPERIMENTS: OBSERVATIONS OF SMOKE DIFFUSION IN THE SURFACE LAYER OVER HOMOGENEOUS TERRAIN

Torben Mikkelsen

Abstract. Instantaneous diffusion estimates have been obtained from observations of smoke plumes in the neutral-unstable planetary boundary layer over homogenous rural terrain.

Ground-level smoke releases were photographed from an aircraft at 1000-6000 feet above the experiment field over 40 min periods. Simultaneously, wind data were recorded from a horizontal array of four tower-mounted sonic anemometer/thermometers (z = 10 m) during periods over which the mean wind direction was virtually perpendicular to the span of the array.

Sufficient data were obtained to evaluate the performance of a small-scale puff diffusion model, as well as the applicability of a recently proposed statistical theory of diffusion of Gaussian puffs.

(continued on next page)

March 1983
Risø National Laboratory, DK-4000 Roskilde, Denmark

The plumes generated by the puff diffusion model showed reasonable agreement with the observed smoke diffusion, and averaged values of the observed cloud spread were found to be comparable with the statistical relative diffusion theory on the ~ 1-km scale considered.

For nu har jeg lært saa vel
Udad lærte Bøger:
At man Stedet uden Skjel
Her paa Heden søger.

St.St. Blicher
(Trækfuglene, 1838)

UDC 551.511

ISBN 87-550-0949-2
ISSN 0106-2840

Risø repro 1983

The present report (Risø-R-479) is part of the thesis:

FORMULATION AND EXPERIMENTAL EVALUATION OF AN OPERATIONAL PUFF DIFFUSION MODEL

submitted to the Technical University of Denmark together with the reports Risø-R-475 and Risø-R-476 in partial fulfilment of the requirements for the degree of lic.techn. (Ph.D.).

Professor K. Refslund acted as responsible supervisor and mag.scient. L. Kristensen functioned as advisor. Professor E. Eliasen was appointed external examiner.

CONTENTS

1. INTRODUCTION

During two experimental campaigns carried out in August 1980 and August 1981, studies of ground-level smoke releases took place over flat moor terrain situated immediately south of the Danish town of Borris in Western Jutland.

The overall purpose of the experimental campaign was to evaluate the theories and principles behind an operational small-scale puff diffusion model (Mikkelsen, 1979, Mikkelsen et al., 1980, Mikkelsen, 1982a and Mikkelsen, 1982b). Specifically, the objective was to investigate experimentally the statistical theory of diffusion of Gaussian puffs, (Mikkelsen, 1982c) as well as to study the applicability of a proposed advection scheme for puffs (Mikkelsen, 1979 ,and Mikkelsen, 1982a), based on a time series of the wind velocity from a single point measurement.

2. THE EXPERIMENT

2.1 Experiment Site

The experiment site was a 1 km × 1 km flat area in the middle of the Borris moors, which are part of a Danish army exercise area. As can be seen from the illustrations in Fig. 2.1 a) and b) the site is ideal for meteorological experiments due to its flatness and homogeneity.

The differences in elevation over the test area, which is to the east of the north-south running dirt road shown in Fig. 2.1, are as small as on the order of 1 metre. The August vegetation consists exclusively of naturally growing grasses and blossoming heather plants, all of which constitute a homogeneously distributed roughness over the terrain of approximately 1 cm.

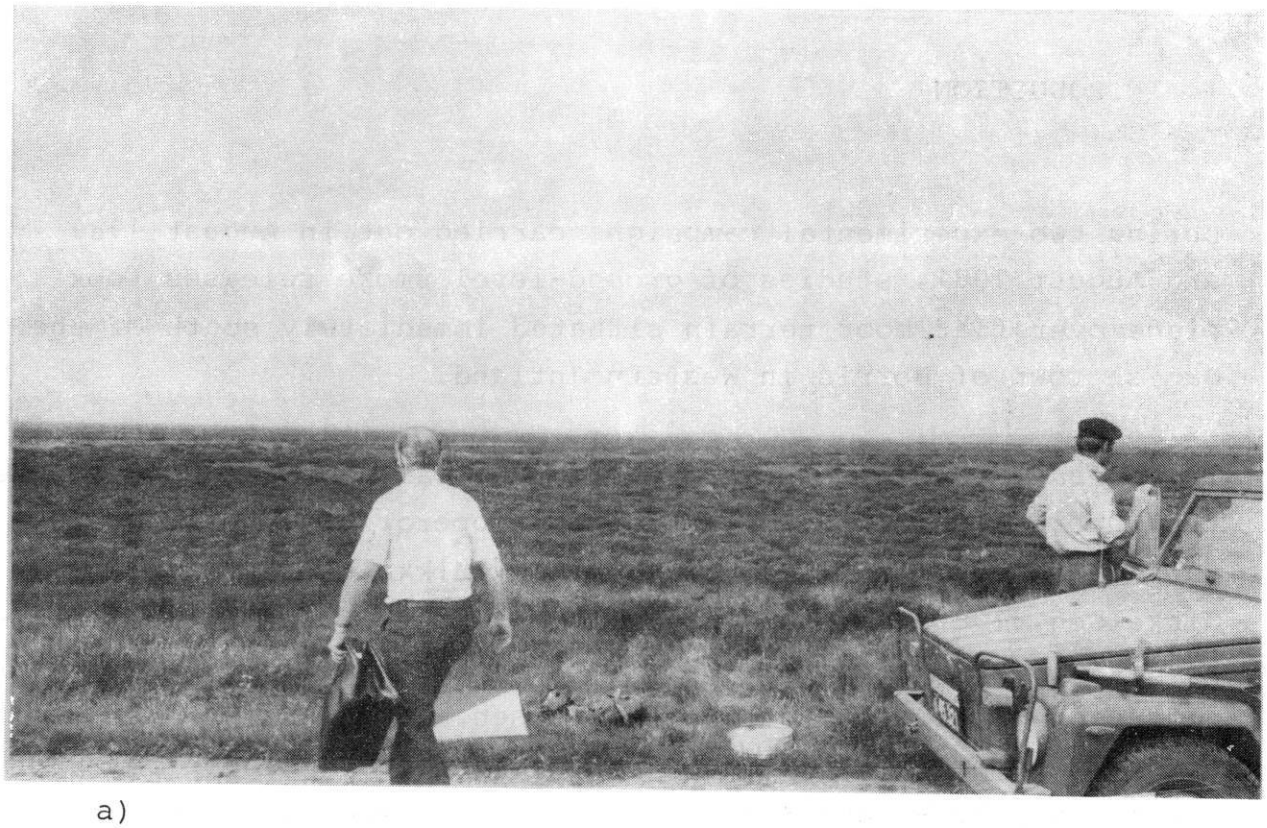

a)

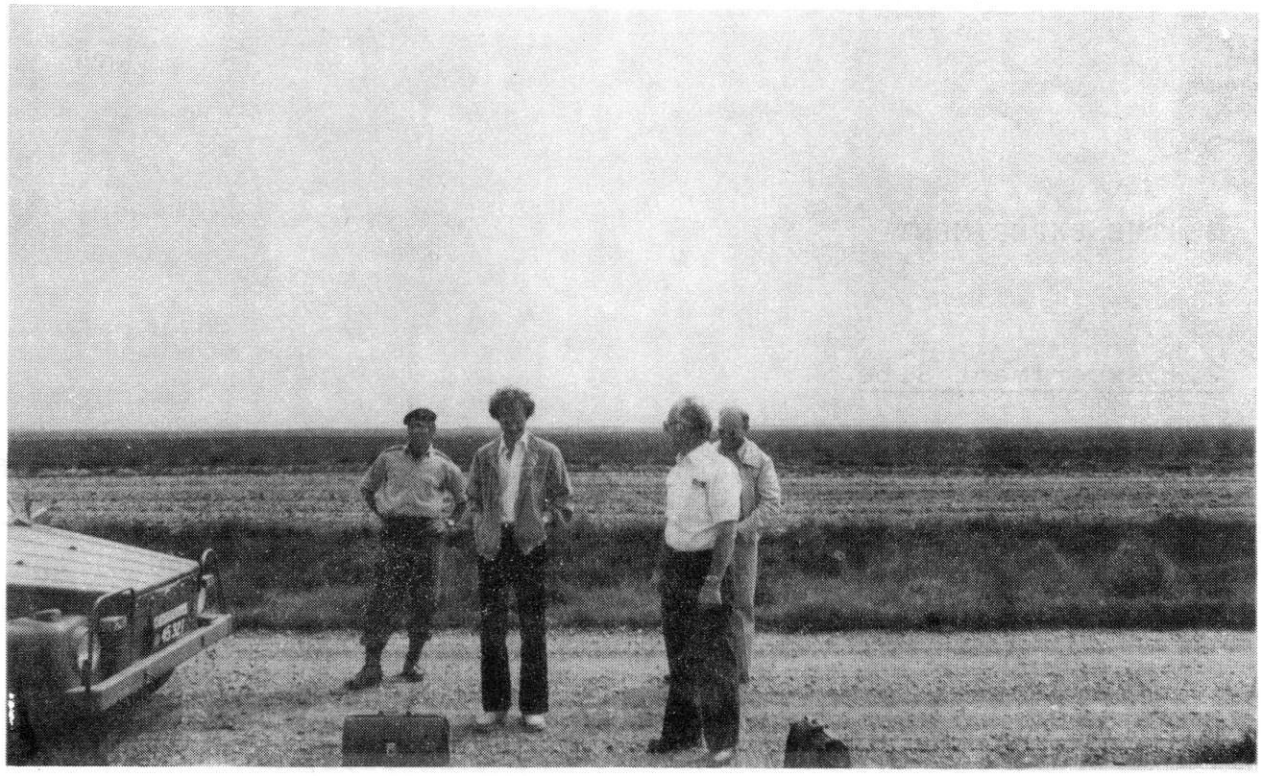

b)

Fig. 2.1. The BOREX experiment site. a) View upwind (looking west) from the smoke release point. b) View downwind (looking east) from the smoke release point. The 4 meteorological masts were erected in the approx. 10-meter wide fire protection belt running parallel to the north-southerly oriented dirt road.

2.2 Meteorological Instrumentation

Four 10-m high meteorology masts were placed in a north-south oriented array perpendicular to the easterly defined downwind direction x (see Fig. 2.2). Each of the 10-m high masts were top-mounted with 3-axis sonic anemometers/thermometers (Kaio Denki type DAT 310). The positioning of the masts (cf. Fig. 2.2) made it possible to obtain estimates of the covariances of all three velocity components with six, approximately logarithmically equidistant, lateral displacements: 4.5 m, 7.5 m, 12 m, 18 m, 25.5 m, and 30 m. In addition, direct monitoring of the wind speed as well as an absolute measurement of the mean direction during experiments were made possible by equipping one of the masts with a sensitive cup anemometer and a calibrated vane near the top of one of the masts.

2.3 Release and Detection of Smoke

As many as four smoke-pots, each containing 10 kilos of the powder Hexit*), were mounted in a stack at the baseline between the masts. When ignited, the smoke-pots produced a visible plume that could be followed from a small aircraft as far as ~ 1 km downwind under light wind conditions. An electrical scale equipped with a strip chart, measured the mass of the smoke stack continuously and thereby also the smoke release rate. In addition, a thermometer, mounted 1 metre downwind from the release point, measured the exhaust temperature of the smoke. At this short downwind distance, the smoke temperature was detected to be surprisingly low, on the average less than ~ 50°C above the ambient air temperature. The low excess temperature of the compound measured can be explained by the high affinity of the hexit gas for the moisture in the atmosphere and a corresponding increased initial entrainment rate. Taking into account the re-

*) Hexit (HC), a mixture of zinc- and clorine-enriched powders. It reacts strongly with the moisture in the atmosphere and forms a thick, white smoke.

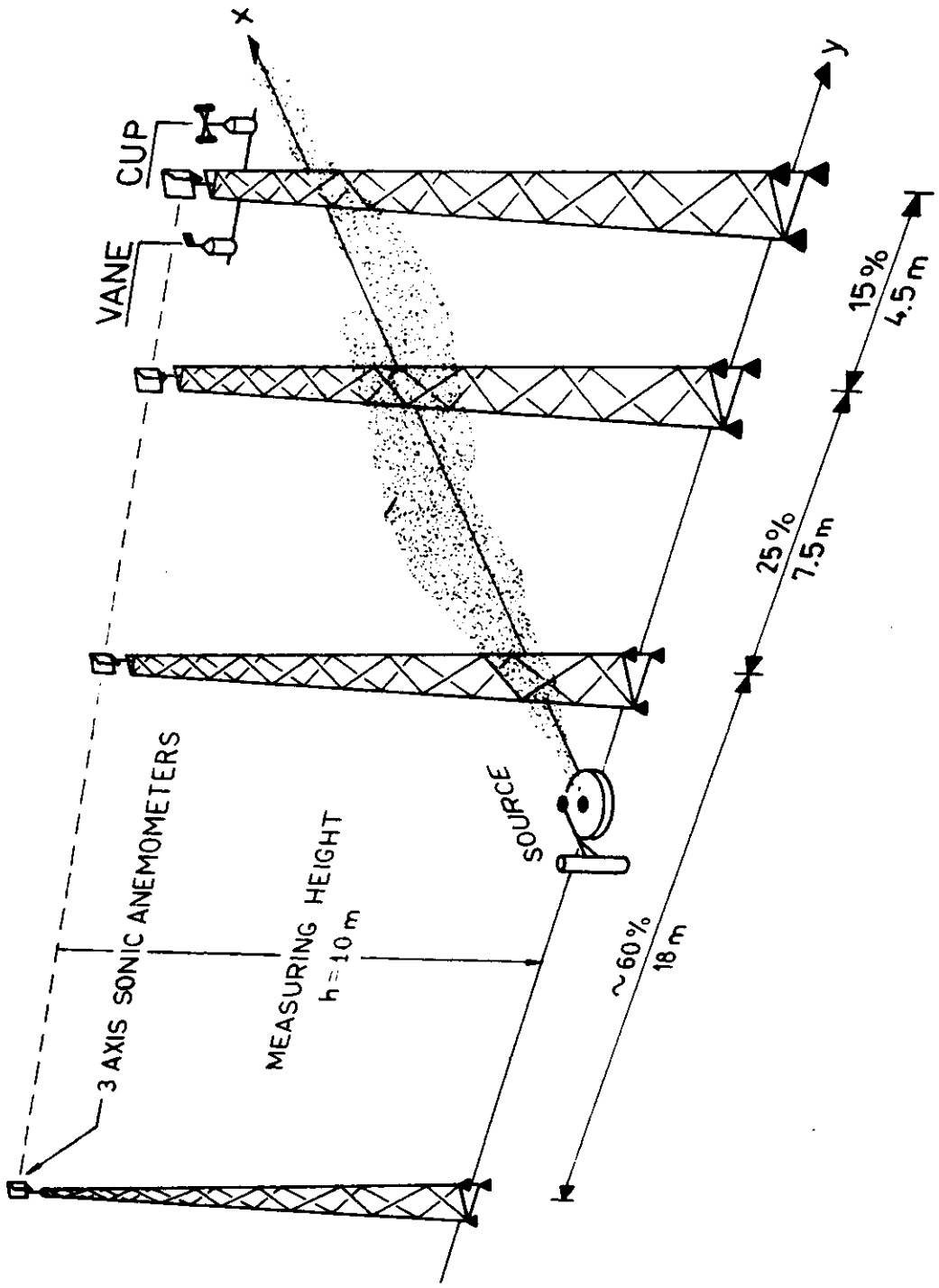
x
y
CUP
VANE
3 AXIS SONIC ANEMOMETERS
MEASURING HEIGHT
h = 10 m
SOURCE
~60%
18 m
25%
7.5 m
15%
4.5 m

latively small volume flux from the source, the buoyancy and subsequent plume rise (approx. 10 metre at x = 1000 m) was deemed to be insignificant relative to the vertical mixing of the smoke in the neutral to unstable atmossphere encountered during the measurements.

The visible contour of the white smoke plume was registered on photographs taken from an airplane against a network of white contrast plates, which were placed on the ground in crosswind-oriented lines at downwind distances of 31.25 m, 62.5 m, 125 m, 250 m, and 500 m. The spacing between the contrast plates was 5 metres at the first three downwind distances, 10 metres at the 250-m line and 20 metres at the 500-m downwind distance.

Figure 2.3 shows a picture taken of the smoke release from a position ~ 1000 feet over the source point. The visible contour of the smoke plume is seen to be easily detectable, and its position can be measured against the white contrast plates, placed on the ground below.

The 35-mm camera used for the recordings was equipped with either a 18-mm wide-angle (100^{o}) objective or a 50-mm (47^{o}) objective depending on the height of the aircraft. In addition, the camera had a timer which marked the pictures with the exact time and date of the exposure. The high-winged Cessna aircraft used during the experiments is shown standing on a nearby air-

---

Fig. 2.2. The meteorological instrumentation. With the individual positioning of the four masts as shown, velocity covariances could be obtained with the following lateral displacements: 4.5, 7.5, 12, 18, 25.5, and 30 meters. The smoke was released at the position between the first two masts as indicated.

Each of the 4 masts was top mounted with Kaijo Denki DAT 310 three-axis sonic anemometer and thermometers.

The downwind direction in the figure (x) points easterly whereas the lateral direction y points southerly, parallel to the dirt road shown in Fig. 2.1.

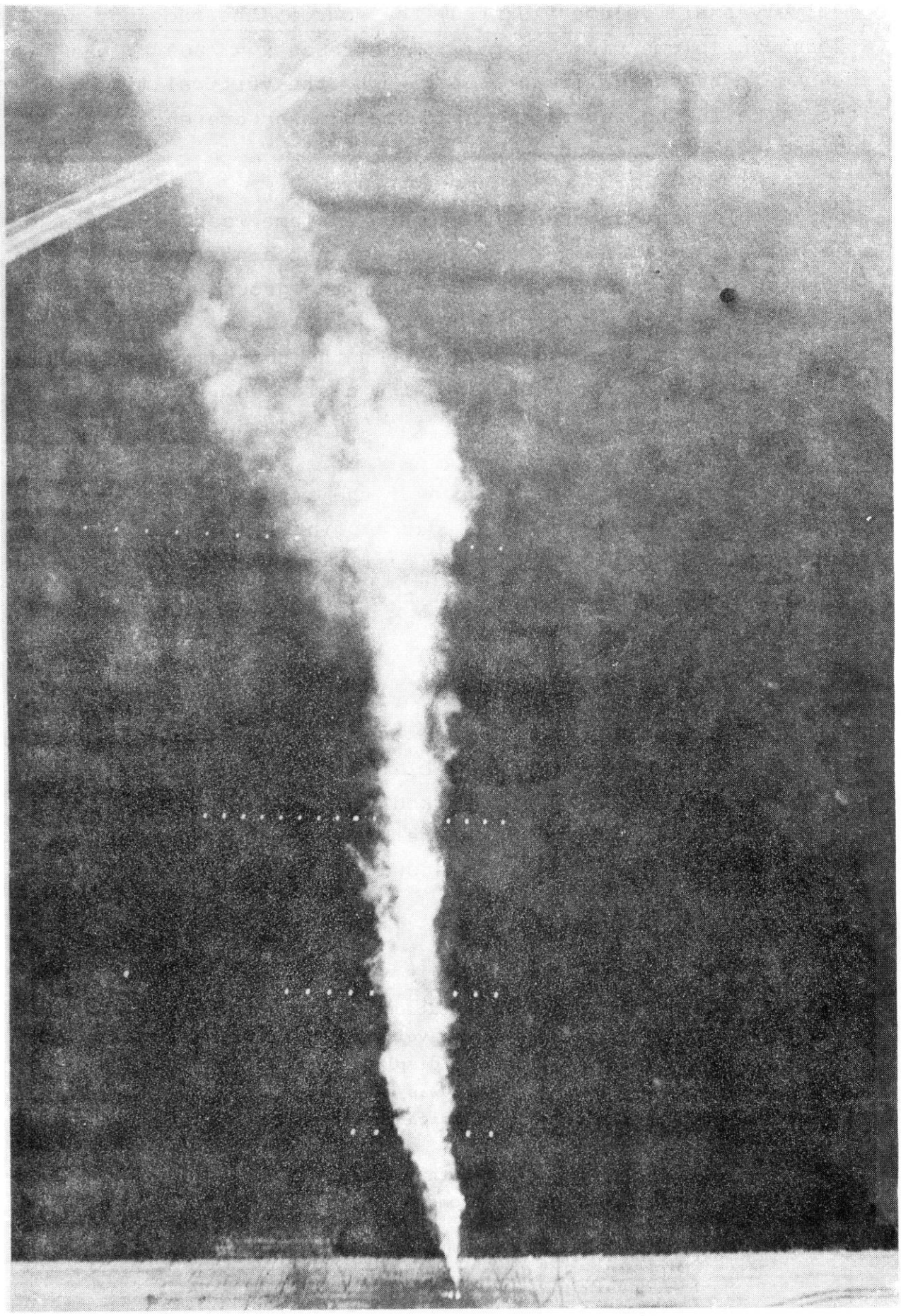

field in Fig. 2.4. A special flying technique was developed in order to compensate for the drift of the plane with the mean wind, and in this way a picture of the visible smoke plume could be taken from above the source point approximately every other minute. A series of approximately 20 pictures could be obtained in this way during each 40-min release experiment.

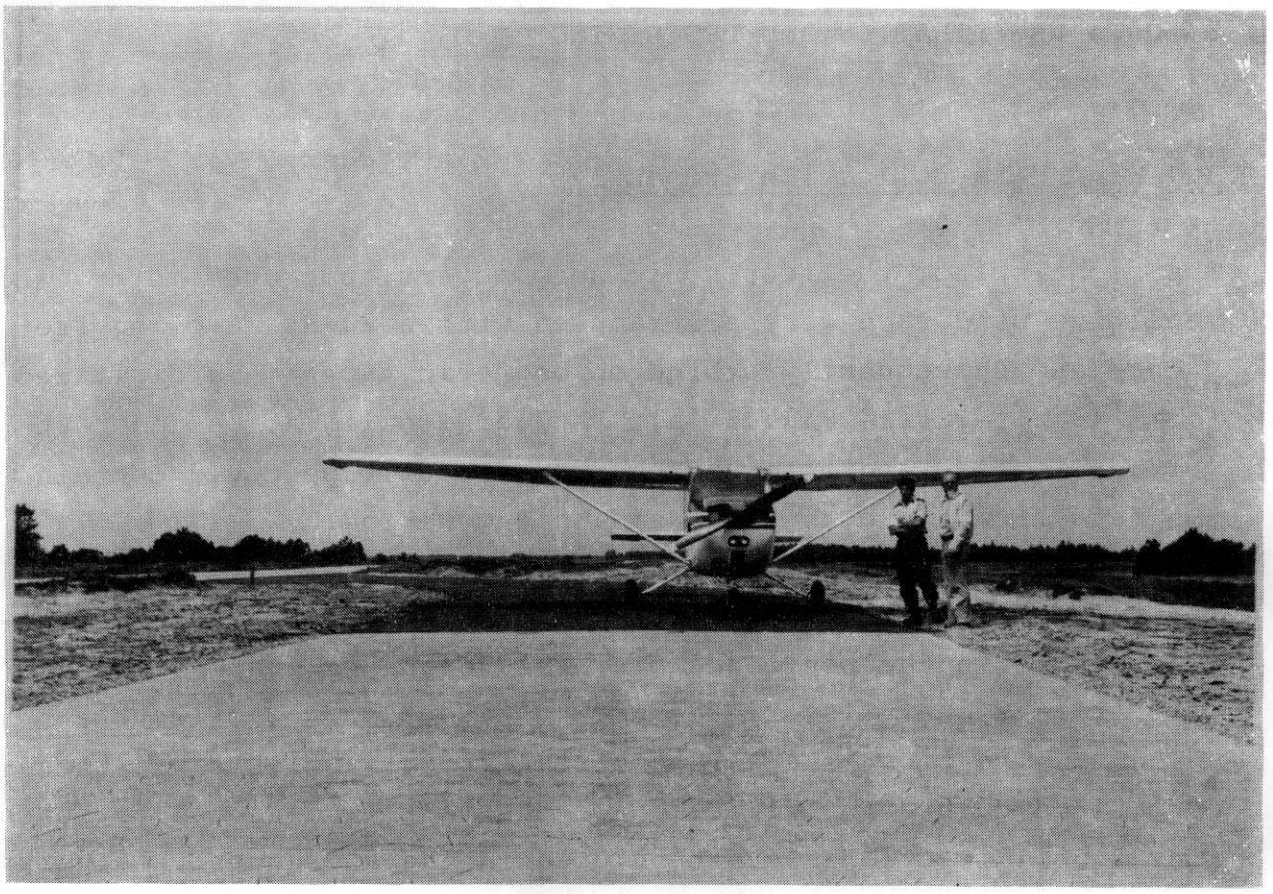

Fig. 2.4. Aircraft used during the BOREX experiments.

Fig. 2.3. Air photo of the instantaneous smoke plume taken from approximately 1000 feet above the source point. The white contrast plates constitute a network of lines normal to the x-axis at the following downwind distances: 31.25 m, 62.5 m, 125 m, 250 m and 500 m. Their lateral spacing is 5 m in the first three rows, 10 m in the 250 m row, and 20 m in the 500 m row.

At least one and sometimes two radio-sondes were launched during each experiment from which information was gained about the wet and dry bulb temperature profiles of the atmosphere. This in turn gave information about the stability and mixing height of the boundary layer.

3. DATA REGISTRATION AND PROCESSING

3.1 Wind data collection and analysis

The signals from the four sonic anemometers, cup anemometer, and sensitive wind vane were all sampled with a 20-Hz sampling frequency and subsequently stored on magnetic tapes in a digitized form (12 bits) (see Fig. 3.1a). Including calibration and test-voltages before and after a recording, each tape could contain the data from a 3-h continuous sampling period.

The velocity components stored on the magnetic tape were necessarily those in the sonic anemometers' reference system, since prior to the analysis, the mean wind direction was of course unknown. The first stage in the statistical analysis was therefore to calculate the direction of the mean wind vector for each run. These directions were then used in the subsequent analysis to rotate (first about the vertical, then about the lateral anemometer axis) the measured components into a reference frame with the x-axis along the mean wind direction and the y-axis in the horizontal plane. The resulting longitudinal (u), lateral (v), and vertical (w) velocity components were thereby oriented so that $\bar{u} = U$ and $\bar{v} = \bar{w} = 0$.

Data were processed with the data analysis programs shown in Fig. 3.1b. The Sonic-alignment Program processes the sonic anemometer data from an arbitrarily chosen 54.6-min period (2^{16} data points) into calibrated, internally and externally aligned time series. The time series could thereafter be displayed in plots

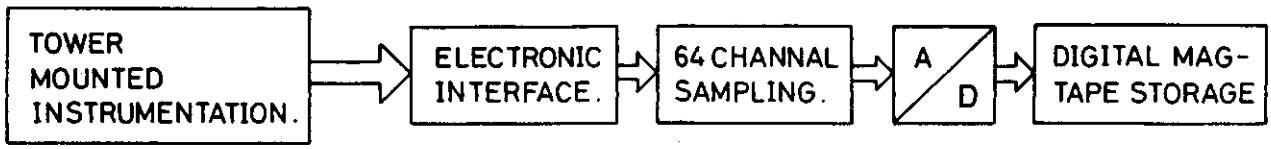

(A) DATA COLLECTION AND STORAGE.

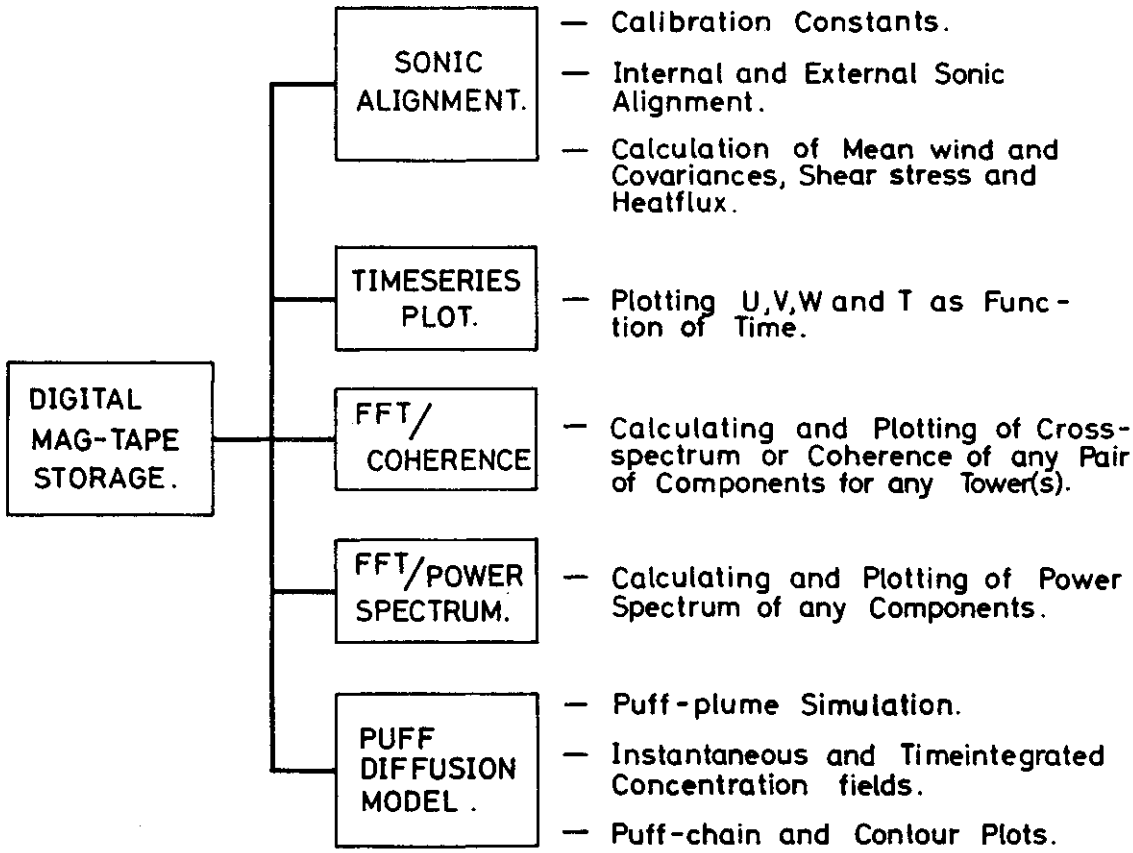

(B) DATA ANALYSIS PROGRAMS.

Fig. 3.1. Block diagram of data collection and analysis system.

and linear trends could be removed. Subsequently power spectra and coherences could be calculated with the different codes shown in Fig. 3.1b.

The branch of the program "FFT/Power Spectrum" provides a direct FFT-calculation on the untruncated time series (2^{16} points). Coherences and their corresponding phases were calculated with the algorithm "FFT/ Coherence". The 2^{16} data point time series

were first divided into eight 2^{13} data point time series. Coherences (and also power spectra) were then calculated from an ensemble average of the spectral amplitudes from each of the eight subintervals.

A further possibility was to use the calibrated time series from the anemometer positioned closest to the smoke pot as a drive for Risø puff diffusion model referred to in the introduction. In this way it was possible to simulate the smoke diffusion scenario with a chain of sequentially released Gaussian puffs.

3.2. Smoke data collection and analysis

During each of a total of 10 smoke-accompanied runs, approximately 20 pictures similar to that in Fig. 2.3 were taken over the source point from the small airplane at intervals of approximately 2-min duration. The cruising altitude of the air-plane varied from experiment to experiment between 1000 and 6000 feet, depending on the height of the cloud base and on the overall visibility of the atmosphere. High-altitude pictures produced less distortion of the experiment site on the film plane in the camera, but they also resulted in reduced contrast due to moisture and dust in the air. The aircraft height above the source point was measured with the plane's altimeter. However, this could also be inferred from measuring the distance δ between the marker plates on the film and by use of the formula $h = f_o(D/\delta)$, where f_o is the focal length of the objective and D the distance between the marker plates on the ground. By comparing the outline of the plume with the ground-positioned marker plates on the pictures, it was possible to determine the lateral visible contour of the smoke plume as a function of the distance from the source point. By subsequent use of the opacity method (Gifford, 1980), the corresponding lateral standard deviation σ_r of the instantaneous plume could be inferred by assuming an instantaneous Gaussian displacement distribution function for the smoke particles. With a constant release rate, the relation between the visible half-width y_c and the instantaneous standard deviation σ_r of the smoke cloud is (Gifford, 1980)

$$\sigma_r = y_c/\{\ln(ey^2_{c,max}/\sigma_r^2)\}^{1/2} \qquad (3.1)$$

where the quantity $2y_{c,max}$ denotes the maximum visible contour width of the smoke plume and e is the base to the natural logarithm. This equation is plotted in Fig. 3.2. When Eq. (3.1) is used in the limit for $y_c << y_{c,max}$ only, the set of curves plotted in Fig. 3.2 shows that the relation between σ_r and y_c is rather insensitive to changes in $y_{c,max}$, and therefore to fluctuations in the smoke release rate. The maximum visible plume width, $2y_{c,max}$ was typically between 50 and 100 metres, and was observed at downwind distances between 500 and 1000 metres.

The data processing of the large amount of smoke data was facilitated in the 1981 experiments by digitizing the visible contour positions on a desk-top computer. A plotter used as a digitizer collected the contour data at a number of positions along the plume. Both the plumes instantaneous lateral spread σ_r and its instantaneous lateral position $y_{cm} = (y_c^+ - y_c^-)/2$ (where y_c^+ and y_c^- are the upper and lower contour positions at fixed x, respectively) could automatically be registered in this way at logarithmically increasing downwind distances. Ensemble-averaged standard deviations $\bar{\sigma}_r$ of the relative diffusion have been obtained in this way from individual experiments together with an ensemble-averaged estimate of the plume's centre of mass variance $\overline{y^2_{cm}}$ down to distances of the order of ~ 1 km from the source. With the Gaussian particle distribution assumed in Eq. (3.1), the quantity $\overline{y^2_{cm}}$ can be interpreted as the spreading connected with the center-of-mass movement of the instantaneous plume. The single-particle dispersion Σ referred to the fixed coordinate system y thus has been estimated by the relation $\Sigma^2 = \overline{\sigma_r^2} + \overline{y^2_{cm}}$ (cf., for instance, Mikkelsen 1982c).

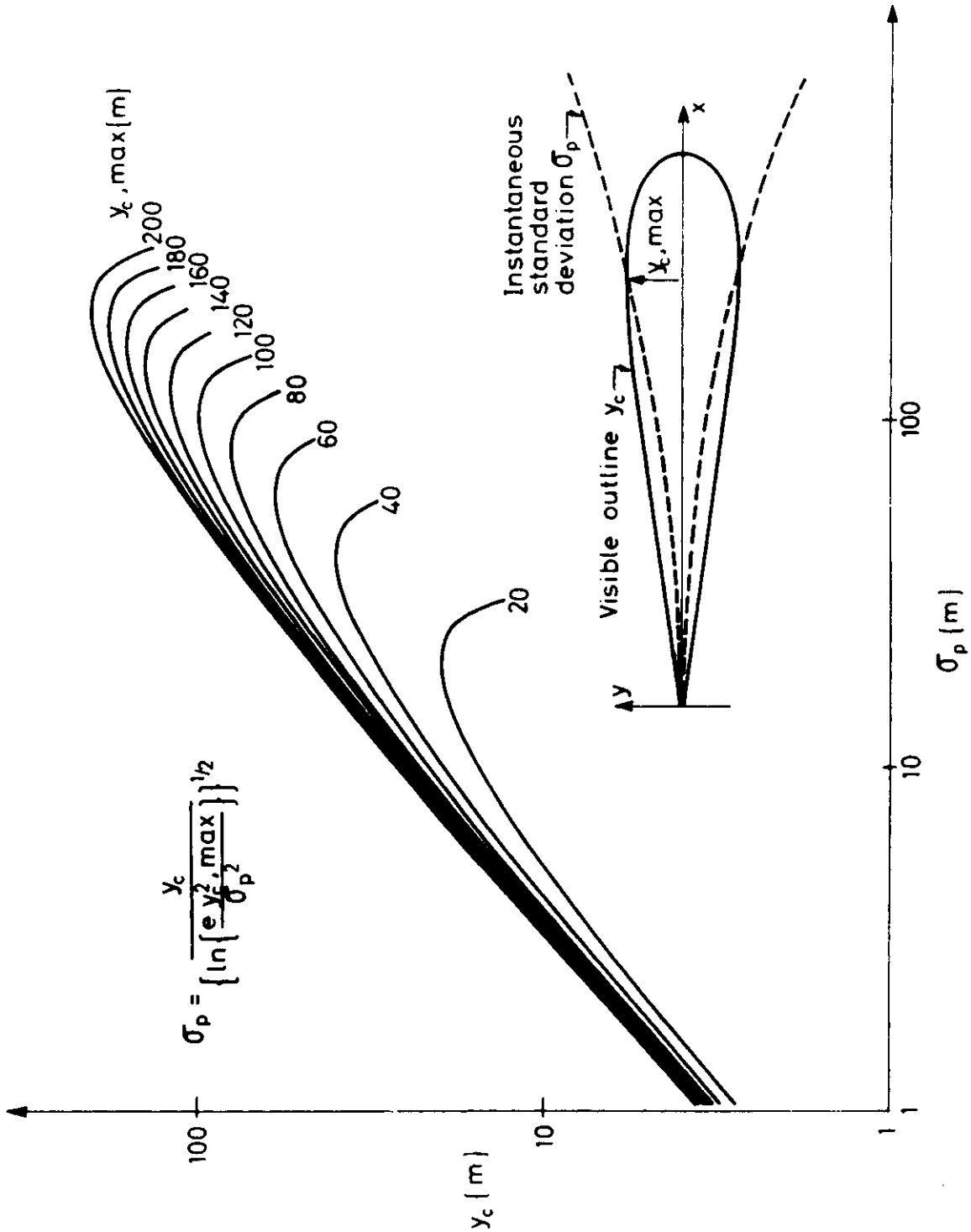

Fig. 3.2. Given the maximum visible width $y_{c,max}$ of an instantaneous plume, the corresponding graph relates an observed width y_c to a corresponding standard deviation of a puff σ_p, by assuming a Gaussian particle distribution of the plume. At the position of maximum visible width, $\sigma_p = y_c = y_{c,max}$ as shown in the inserted figure. At shorter distances, $y_c > \sigma_p$, whereas at larger distances $y_c < \sigma_p$. The "opacity" method, Gifford (1980), can be used with accuracy only when $y_c << y_{c,max}$.

4. RESULTS AND DISCUSSION

4.1 Calibration experiments (MOLEX)

In order to calibrate the four sonic anemometers and to check the data-analysis programs in Fig. 3.1b, an array of 3-m high masts, with spacing similar to that shown in Fig. 2.2 was set up in the Roskilde Fjord in shallow water close to the Risø peninsula. The effective anemometer height over the water surface was of the order of 2 metres.

Wind data from two 2^{16} data point runs, which corrresponds to a ~ 56-min sampling period with a 20-Hz sampling frequency, will be discussed here. The first of these was taken under unstable conditions, the other during neutral conditions.

MOLEX run 7

This run took place during an afternoon in mid-August with the wind coming out of the west perpendicular to the mast array at approximately 3-4 m/s. The sun was shining from an almost clear sky (1/8 cloud cover) and the surface wet and dry bulb temperatures were 15.5^{o} and 19^{o}C, respectively (RH = 70%). The water surface temperature upwind from the mast was 20.2^{o}, which was taken as an indication of a somewhat unstable surface layer. In Fig. 4.1 velocity spectra are shown obtained for the three components, u, v and w, for each of the four masts, calculated by the program FFT/COHERENCE. An inertial subrange with a $k^{-5/3}$ dependency is evident in all spectra. In the high wave number end, evidence of local isotropy is present through the 4/3 ratio measured between the longitudinal (u) and the two transverse (v, w) spectral amplitudes. The almost identical shape and amplitude of the spectra of the four different anemometers seem to justify the calibration and alignment procedures used.

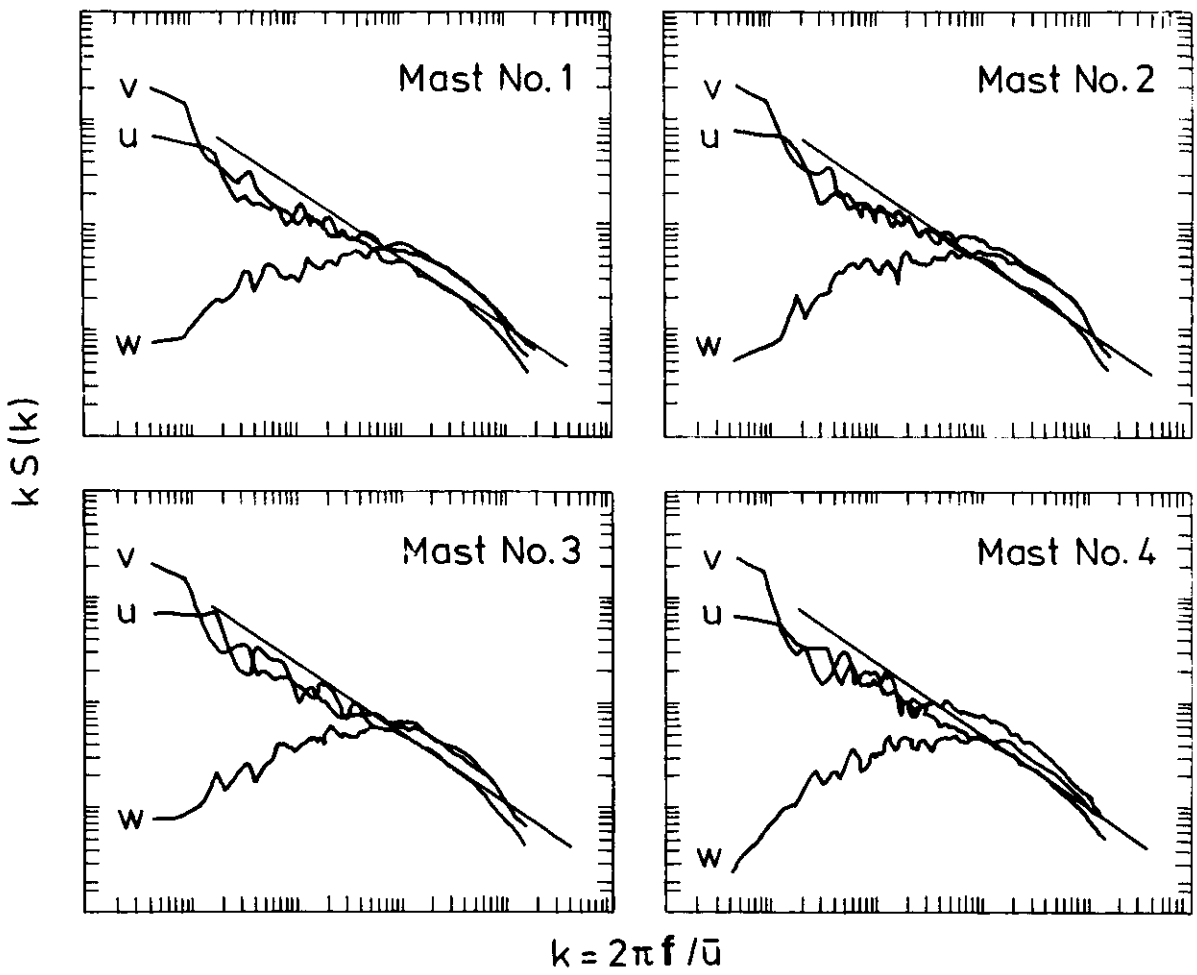

Fig. 4.1. Power spectra as function of wave number, kS(k), of the three velocity components u, v, and w for each of the four sonic anemometers used in the calibration experiment MOLEX RUN 7. The wavenumber k is related to the frequency f by: $k = 2\pi f/\bar{u}$. The full line shown has slope equal to -2/3.

Plot of spectrum	MOLEX/FFT/RUN 7
spectrum multiplied by:	k
Mean wind speed U:	3.50 m/s
Number of raw estimates:	4096
Sampling period:	0.050 secs
Relative bandwidth:	0.20
Range of k:	10^{-3}, 10
Range of ordinate:	10^{-4}, 1

Table 4.1 presents the mean and turbulence data obtained. From the sonic anemometer/thermometers an average value was found for the Monin-Obukhov stability length L, which in terms of the total heat flux $\overline{\theta'\omega'}$ *) and the friction velocity u_* reads

$$L = \frac{T}{\kappa g} u_*^3 / \overline{\theta'w'} \quad . \tag{4.1}$$

Here T is the average surface layer temperature, g the constant of gravity, and κ the von Kármán constant. The Monin-Obukhov length found (of the order of -10 m) is characteristic of a rather unstable boundary layer, in accordance with the temperature difference measured.

Table 4.1. Calibration experiment (MOLEX RUN 7).

MAST No.	U	$\overline{u^2}$	$\overline{v^2}$	$\overline{w^2}$	$\overline{\theta^2}$	u_*	L
	m/s	m^2/s^2	m^2/s^2	m^2/s^2	K^2	m/s	m
1	3.52	0.372	0.715	0.054	0.215	0.18	-13
2	3.76	0.410	0.761	0.051	0.165	0.17	-17
3	3.76	0.432	0.734	0.053	-	0.17	
4	3.79	0.370	0.851	0.044	0.127	0.13	- 7

- data not available

*) The quantity θ' denotes the moisture-corrected virtual temperature, and therefore $\overline{\theta'w'}$ represents the total (latent and sensible heat flux (see Busch, 1973)). Sonic anemometers measure the sound virtual temperature, but for all practical purposes this equals θ' so that an estimate of the total heat flux has been obtained from the sonic anemometer/thermometers (see also Schotanus et al., 1982).

MOLEX run 8

At noon, two days after the MOLEX run 7 experiment was performed the wind again came out of the west perpendicular to the mast array. Due to an almost total cloud cover (7/8) and wind speeds in excess of 5 m/s, the stability here was expected to be closer to neutral.

Figure 4.2 shows velocity spectra obtained in a way similar to Fig. 4.1. Here, however, the spectra are shown in three dif-

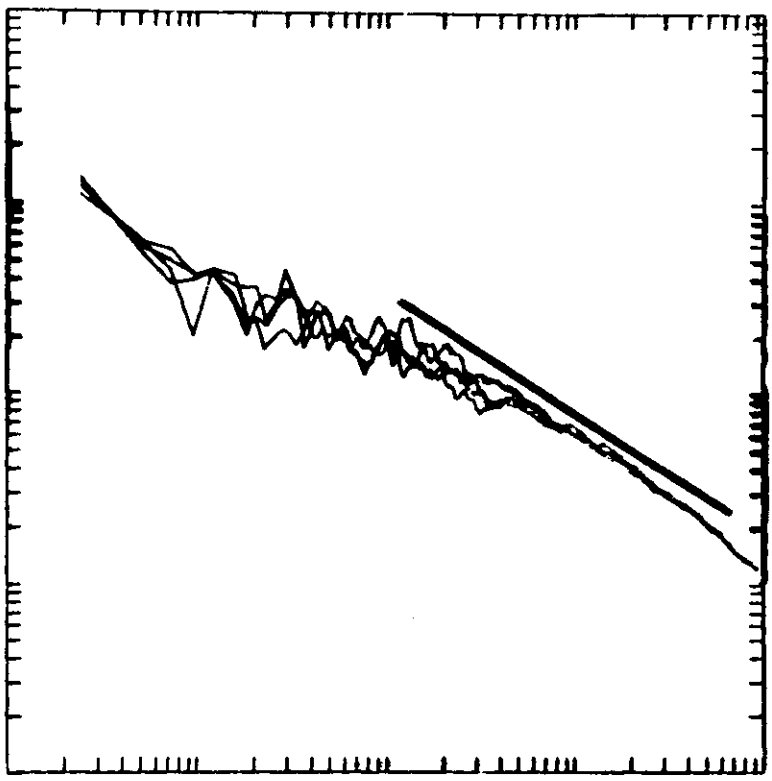

Fig. 4.2a. Power spectra, fS(f), here shown as a function of frequency f, of the four u-components obtained from the sonic anemometers in the calibration experiment MOLEX RUN 8. The full line shown has slope equal to -2/3.

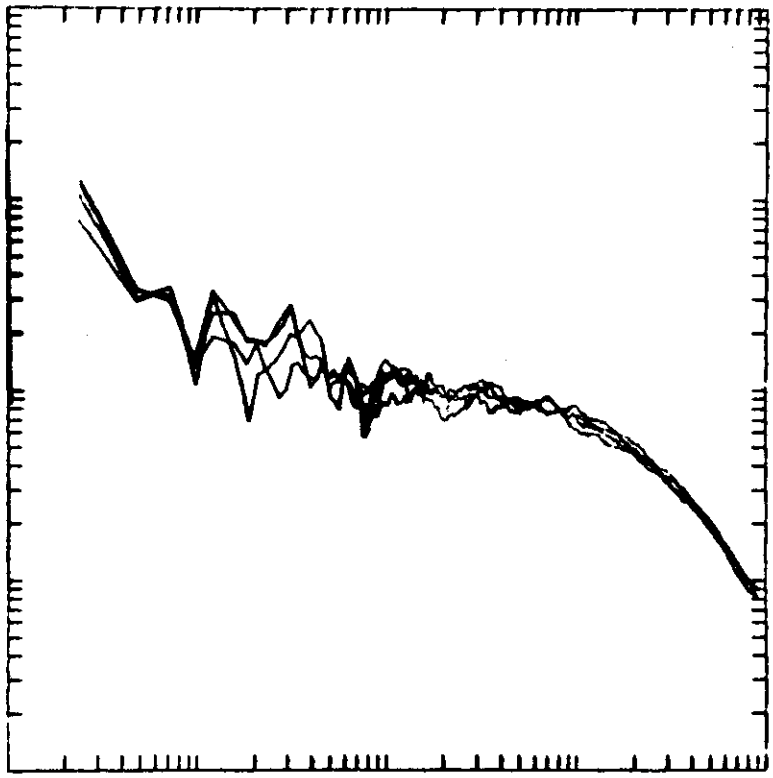

MOLEX.RUN 8.V.

NUMBER OF RAW ESTIMATES : 4096
SAMPLING PERIOD : 0.050 SECS
RELATIVE BANDWIDTH : 0.20
RANGE OF f : 10^{-3}, 10
RANGE OF ORDINATE : 10^{-4}, 1

Fig. 4.2b. As in Fig. 4.2a, but for the four v-components measured.

ferent groups, one for the longitudinal (u), one for the transverse (v) and the last one for the vertical (w) component. The representation in Fig. 4.2 facilitates a direct comparison between the four component spectra.

As in Table 4.1, Table 4.2 summarizes the key data obtained during this run. The Monin-Obukhov length L exhibits some variation from mast to mast, but the average value (of the order of 100 metres) indicates that the stability of the surface layer is close to neutral, or only slightly unstable.

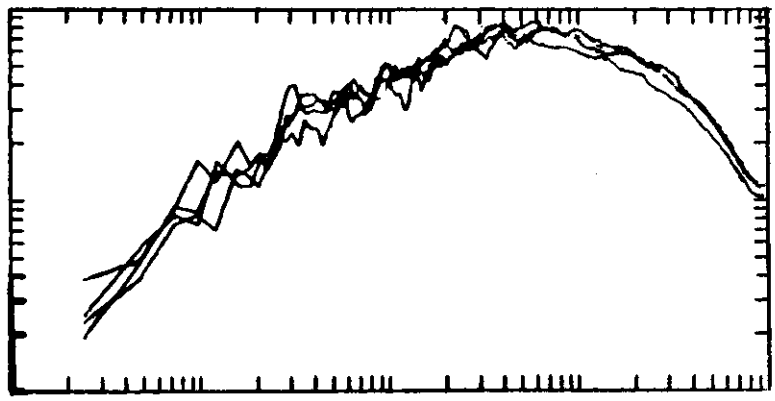

MOLEX.RUN 8.W.

NUMBER OF RAW ESTIMATES : 4096
SAMPLING PERIOD : 0.050 SECS
RELATIVE BANDWIDTH : 0.20
RANGE OF f : 10^{-3}, 10
RANGE OF ORDINATE : 10^{-4}, 1

Fig. 4.2c. As in Fig. 4.2a, but for the four w-components measured.

Table 4.2. Calibration experiment (MOLEX RUN 8)

MAST No.	U	$\overline{u^2}$	$\overline{v^2}$	$\overline{w^2}$	$\overline{\theta^2}$	u_*	L
	m/s	m^2/s^2	m^2/s^2	m^2/s^2	K^2	m/s	m
1	5.10	0.589	0.442	0.061	0.031	0.200	- 54
2	5.37	0.577	0.432	0.065	0.022	0.198	-209
3	5.36	0.563	0.380	0.065	-	0.185	-
4	4.92	0.515	0.313	0.051	0.030	0.185	- 42

- data not available

In Fig. 4.3 the cross correlations $\rho_i = \overline{u_i(y)u_i(y+D)}/\overline{u_i^2}$, (i = 1,2,3) of the three velocity components u, v, and w are shown, obtained with the six possible different values of the lateral displacements D. The observed tendency for finding higher cross-correlation values at fixed displacements during the unstable

Run 7, relative to the neutral Run 8, was found in later experiments as well, and seems to be of a more general character. This increase in cross-correlation at fixed lateral displacements can properly be explained in terms of the larger eddy structure one would expect to be present when warm thermals are produced at the surface and rise up through the surface layer.

The benefit of the total of eight calibration experiments (MOLEX 1-8) carried out at Risø National Laboratory significantly improved the operation and calibration procedures of the four sonic anemometers, and also supported the development and testing of the different data analysis programs used.

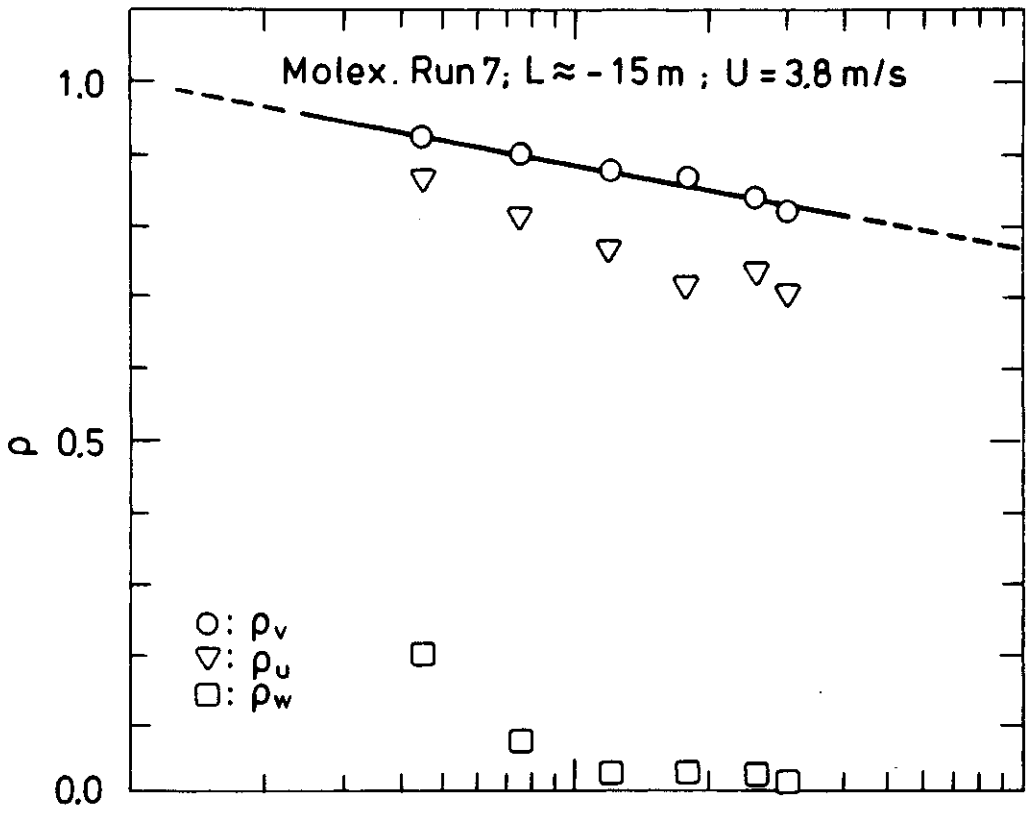

Fig. 4.3a. Cross-correlation coefficients ρ of the three velocity components u, v, and w measured during the unstable stratified MOLEX RUN 7 experiment as function of lateral displacements D. The line fitted through the six measured values of the v-correlations coefficient has the form: $\rho_v = 1 - 0.165 \log_{10}(D)$.

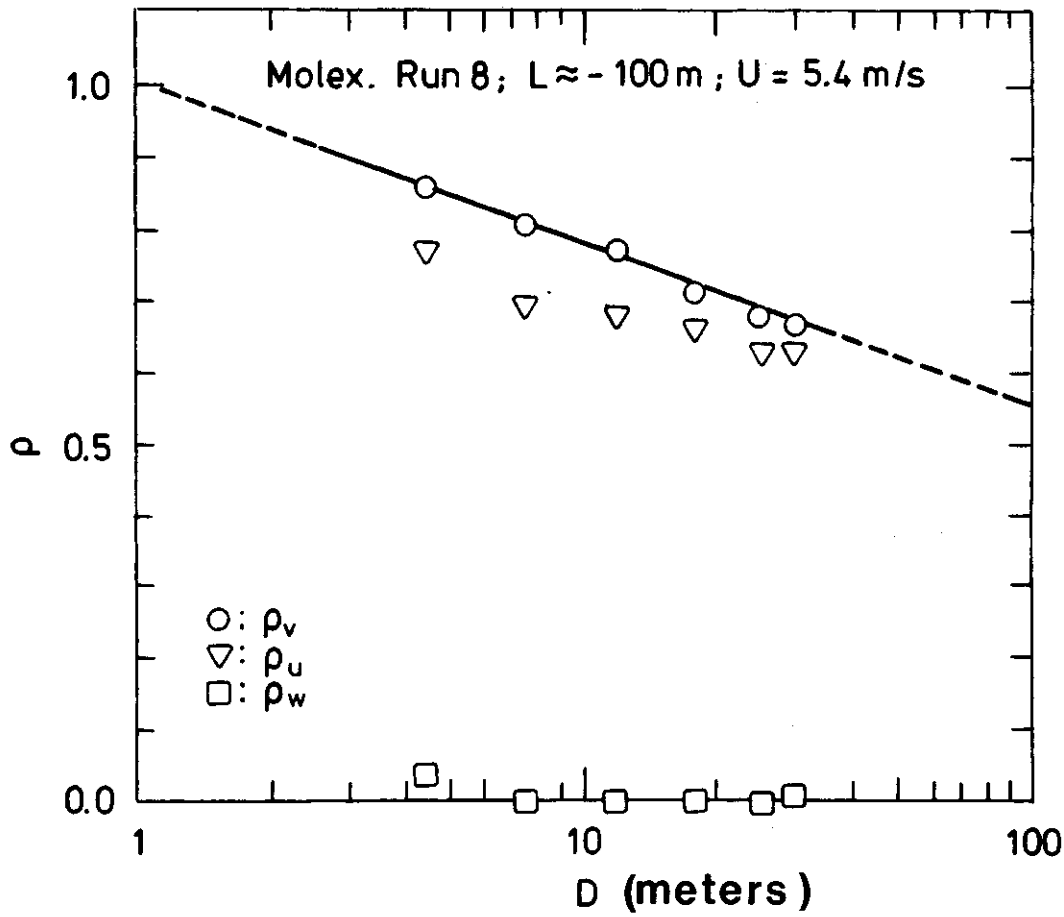

Fig. 4.3b. As Fig. 4.3a, but for the more neutral stratified experiment MOLEX RUN 8. The fitted correlation is here: $\rho_v = 1 - 0.22 \log_{10}(D)$.

4.2 The smoke release experiment BOREX 80 run 6

The 1980 experimental campaign took place at the Borris Sönderland moors in Western Jutland over the period August 24 to 30.

In the middle of the afternoon on Thursday the 28, the sky was almost totally clear and light winds of the order of 4-5 m/s indicated rather unstable atmospheric conditions. A 45-m high meteorological tower, kept in operation by the Danish army two km north of the experiment site yielded a gradient Richardson number $R_i = g/T\ (\Delta\theta/\Delta z)/(\Delta\bar{u}/\Delta z)^2 \cong -1/15$, based on the temperatures at z = 22 metres and z = 2 metres, and a mean wind speed $\bar{u}$ measured at z = 10 metres. By referring to a mean height $\bar{z}$ equal to 10 metres and setting $R_i = \bar{z}/L$, an estimate of the Monin-Obukhov stability length L of ~ -150 metres was obtained. During

the 56-min sampling period, the mean wind speed was determined to be 4.72 m/s, and the longitudinal (u) and lateral (v) variances were, after a linear trend had been removed, 0.62 m^2/s^2 and 0.98 m^2/s^2, respectively.

At the experiment site, the surface temperature (z = 1 metre) reached 20.4° C at 3 p.m. and the relative humidity at that time ~ 57%. During the afternoon, the mean wind direction slowly turned clockwise and at 3.20 p.m., the wind came from the west in an almost perpendicular direction relative to the mast array. Smoke was then released continuously over a 40-min period, and the subsequent analysis showed that the mean wind direction differed by only some 8°-10° from the predefined downwind direction over this period. Between 3.20 and 4.00 p.m., a series of 22 pictures were taken from approximately 1000 feet above the release point, at approximately 2-min intervals. In this experiment, the instantaneous contour and lateral position of the smoke plume could be detected downwind in several pictures as far as ~ 1 km from the source. The smoke data obtained at downwind distances greater than 500 meters were, however, somewhat uncertain.

By referring to the ground-placed contrast plates, it was possible to calculate the instantaneous lateral visible width of the smoke plume, and the corresponding instantaneous (lateral) standard deviations, σ_r, by use of the opacity method described in Section 3.2.

Figure 4.4 presents the ensemble of instantaneous standard deviations σ_r observed as a function of the downwind distance. A considerable scatter in the data at fixed downwind position is to be expected in connection with the turbulent diffusion process considered, and should not be taken as representative of the uncertainty of the measurements. By averaging the observed instantaneous σ_r values at each downwind distance, an average standard deviation of the instantaneous spread $\overline{\sigma_r}$ can be obtained as a function of the downwind distance x.

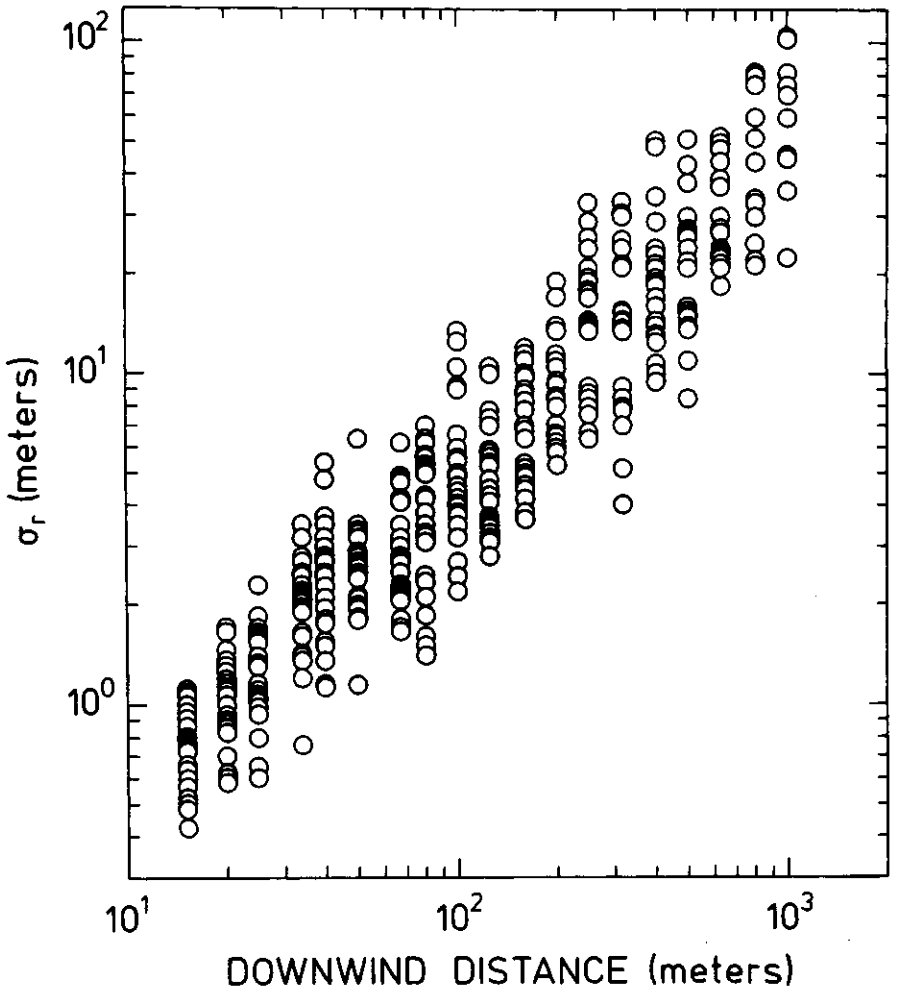

Fig. 4.4. Observed instantaneous standard deviation σ_r during BOREX 80 RUN 6, as function of the downwind distance x.

Figure 4.5 shows the averaged standard deviation $\overline{\sigma_r}$ together with the centroid dispersion $\overline{y_{cm}^2}$, which, as mentioned earlier, can be obtained from the smoke data by assuming a symmetric particle displacement distribution of the smoke plume. The latter is by definition related to a coordinate system aligned with the mean wind direction over the 40-min period and not to the predefined x-axis in Figs. 2.2 and 2.3.

Also shown in Fig. 4.5 is the total lateral dispersion corresponding to Taylor's (1921) theoretical analysis of single-particle diffusion $\Sigma = (\overline{y_{cm}^2} + \overline{\sigma_r^2})^{1/2}$; this is seen to be dominated entirely by $\overline{y_{cm}^2}$ at the downwind positions and for the 40-min sampling period considered.

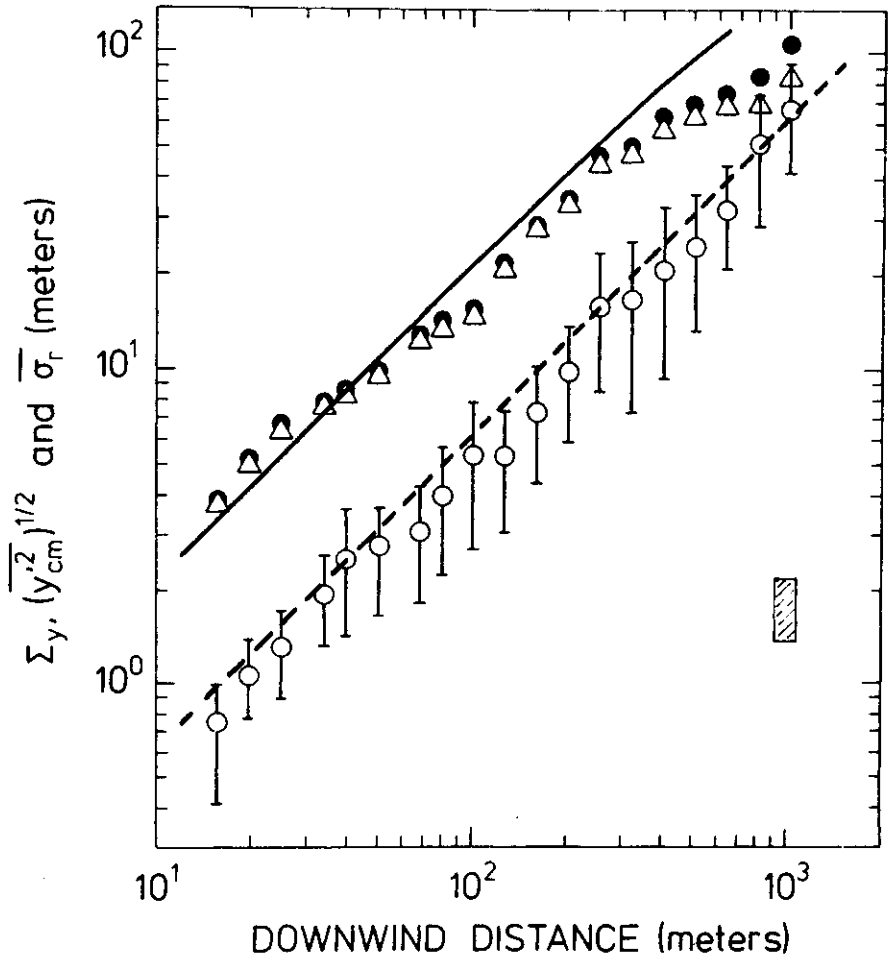

Fig. 4.5. Ensemble-averaged standard deviation $\overline{\sigma_r}$ of the instantaneous observed spreads in Fig. 4.4 versus the downwind distance x. The crossbars through the datapoints represent the standard deviation of the ensemble of instantaneously observed spreads at a particular downwind distance. Dispersion associated with the movement of the centerline of the instantaneous plume, $(\overline{y^2_{cm}})^{1/2}$, has been indicated by Δ, The total (single particle) dispersion Σ_y which is referred to a fixed coordinate at the ground, is indicated by •. The upper solid line is calculated on the basis of Taylor's (1921) absolute diffusion theory: $\Sigma_y = i_v x$, whereas the stipled line has been drawn from the formula given by Smith and Hay (1961) for the expansion of a three-dimensional isotropic Gaussian puff: $\sigma_p = 0.22\ ix$.

The shaded vertical bar, which is inserted in the lower right corner of the figure represents the statistical uncertainty (± one standard deviation) on the estimate of $\overline{\sigma_r}$.

The average standard deviation of the instantaneous spread in Fig. 4.5 is found to a first approximation to grow linearly with the downwind distance. However, some scatter in $\overline{\sigma_r}$ between the logarithmically equidistant (increment factor = $2^{1/3}$) downwind distances is present, and is most probably a consequence of statistical uncertainty due to the relatively small ensemble of 22 pictures. It is reasonable to assume that smoke plumes observed at two-minute intervals represent independent outcomes of the stochastic diffusion process that is responsible for the instantaneous width of the plume. At least this must be true for the downwind distances considered here, since the smoke particles observed on individual pictures all have been advected out of the experiment site during the time period between two photographs. The statistical uncertainty, $\Delta\overline{\sigma_r}$, of the estimated average spread of $\overline{\sigma_r}$ is therefore of the order $\sim\sqrt{22}/22 = 21\%$. In Fig. 4.5 the shaded bar shows the 68% confidence level ($2\Delta\overline{\sigma_r}$) of $\overline{\sigma_r}$, and it is seen that most of the observed scatter in $\overline{\sigma_r}$ can be explained in terms of this.

At distances shorter than ~ 500 metres, the observed values of $(\overline{y'^2_{cm}})^{1/2}$, and thereby also of the absolute or fixed frame diffusion Σ, are found to increase linearly with the downwind distance. Here, however, the scatter about a straight line fitted to the observations seems to be more correlated and systematic from point to point. But the stochastic process responsible for the advection and positioning of the plume over the experiment site is also of a different character than that responsible for the instantaneous width of the plume. The plume advection has to do with the more energetic structures or eddies of the turbulence that exist on the scale comparable with the experiment site (cf. the discussion of the lateral velocity spectrum below). The positioning of the smoke plume in two consecutive observations will therefore not be independent to the same extent as the observations of the instantaneous width, and this may explain the more correlated departures in the scatter observed in Σ.

At distances greater than 500 metres, the observed values of absolute and instantaneous spread seem to converge, but both

the plume location technique, as well as the opacity method used, are rather uncertain at these distances, and not much confidence should be allocated to these measurements.

The topmost curve which falls close to the observations of the absolute diffusion is calculated by means of G.I. Taylor's (1921) absolute diffusion theory. For travel times that are short relative to the Lagrangian time scale t_L of the turbulence, this theory yields $\Sigma = i_v x$. Here, the lateral turbulence intensity i_v is defined by $i_v^2 = \overline{v^2}/\bar{u}^2$. At distances greater than ~ 100 metres, a first-order correction to the near field formula $\Sigma = i_v \cdot x$ has been made based on an observed Eulerian time scale of the order ~100 s (see below) and a ratio of the Lagrangian to Eulerian time scales $\beta = 4$, together with an exponential Lagrangian autocorrelation function. At x = 1000 metres, where the greatest departure from the straight line occurs, $\Sigma = i_v x$, in Fig. 4.5, this correction amounts to only some 17%, however. The corrected version of Taylor's near field diffusion theory is found to represent the observations in Fig. 4.5 well down to $x \simeq 500$ metres.

The dashed line falling within the scatter in the observations of the instantaneous spread represents a formula for relative diffusion suggested by Smith and Hay (1961). Pasquill (1974) also recommended this formula for the expansion of a Gaussian cloud in a field of isotropic turbulence: $\overline{\sigma_r} = 0.22\ i \cdot x$, where $i^2 = (\overline{u^2}+\overline{v^2}+\overline{w^2})/\bar{u}^2$ is the intensity of the turbulence, based on the total energy of the turbulence. This formula has previously been used in the Risø small-scale puff diffusion model (Mikkelsen, 1979 and Mikkelsen, 1982a). For calculating the dashed curve in Fig. 4.5, however, the intensity i has been determined on the basis of the two horizontal velocity variances only, since the vertical velocity variance $\overline{w^2}$ was unavailable from this particular experiment for reasons to be explained. Taking the dashed curve in Fig. 4.5 as a lower estimate for the instantaneous spread, therefore, the formula of Smith and Hay seems to somehow overpredict the observed spread by, say 25%, in this experiment. But a linear relation between $\overline{\sigma_r}$ and x is found to apply reasonably well over the downwind distances considered.

In contrast to the successful collection of smoke diffusion data during the 1980 experimental campaign, the 64-channel data sampling system previously described had to be taken out of operation the very first day of the experiment due to a severe mechanical breakdown in the system's digital tape recorder. Therefore, calibration voltages and wind data were stored on an 8-track analogous tape recorder for later digitalization and processing.

With only 8 channels available for recording data from the four sonic anemometers/thermometers, it was decided to register only the two horizontal velocity components (u and v) from each of the sonic anemometers. In addition to this trouble, the sonic anemometer in mast No. 4 had electronic problems at the time the right wind conditions showed up for Run 6. (Certainly, the work for an experimentalist can be rather frustrating!)

Table 4.3 gives the relatively small amount of data obtained from the mast array during this run. A gradient Richardson number obtained from a nearby 45-m meteorological mast kept in continuous service by the Danish army, has been transformed into an equivalent Monin-Obukhow length of the order of 150 metres in the table. In view of the rather convective behaviour of the smoke plume observed at the experiment site, both from the airplane and also from the ground, this Monin-Obukhov length is probably biased somewhat toward the neutral limit.

From the three anemometers remaining in operation, the power spectra from Run 6 have been calculated using the program FFT/COHERENCE. The three lateral (v) spectra from mast 1 to mast 3 are shown in Fig. 4.6. In contrast to the 20-Hz sampling rate previously used, the sampling rate here was decreased to 25/4 Hz and the corresponding Nyquist frequency in Fig. 4.6 is therefore 25/8 Hz. The somewhat different spectral values calculated at the high-frequency end of the otherwise evident -5/3 initial subrange may be attributed to the undetermined alignment of the sonic anemometers coordinate system about one axis (the y-axis). This missing alignment results from the inability to register the vertical velocity component.

Table 4.3. Smoke release experiment (BOREX 80 RUN 6)

MAST No.	U	$\overline{u^2}$	$\overline{v^2}$	$\overline{w^2}$	$\overline{\theta^2}$	u_*	L
	m/s	$(m/s)^2$	$(m/s)^2$	$(m/s)^2$	K^2	m/s	m
1	-	-	-	-	-	-	-
2	4.88	0.693	1.130	-	-	-	*)
3	4.73	0.671	0.990	-	-	-	*)
4	4.56	0.516	0.825	-	-	-	*)
MEAN	4.72	0.62	0.98				

- data not available

*) Gradient Richardson Number from nearby 45-m tower: T_{22}, T_2, U_{10}

$R_i = g/T\ (\Delta\bar{\theta}/\Delta z)/(\Delta\bar{u}/\Delta z)^2 \simeq -1/15$

with $R_i \simeq z/L$ and $z = 10$ m: $L \simeq -150$ m

By extrapolating the unstable spectra to frequencies of the order of 1/100 Hz, which is representative of the large-scale eddies in the experiment, an Eulerian integral time scale t_E appropriate for the smoke experiment can be estimated to be $\pi F(1/100)/\overline{v^2}$ ~100 s. Setting $\beta = 4$, the corresponding Lagrangian time scale t_L is estimated to be of the order of ~ 400 s. With a mean wind speed equal to 5 m/s, the corresponding length scale, separating the near and the far field limit of the absolute diffusion in Fig. 4.5, is estimated to be ~2 km.

In Fig. 4.7 the measured cross-correlation coefficients of the two horizontal velocity components u and v are shown at the three possible different lateral displacements in Run 6. Experience based on the calibration experiments, and on the 1981 experimental campaign as well, has shown that the measured horizontal cross correlation coefficients ρ fit rather well to ana-

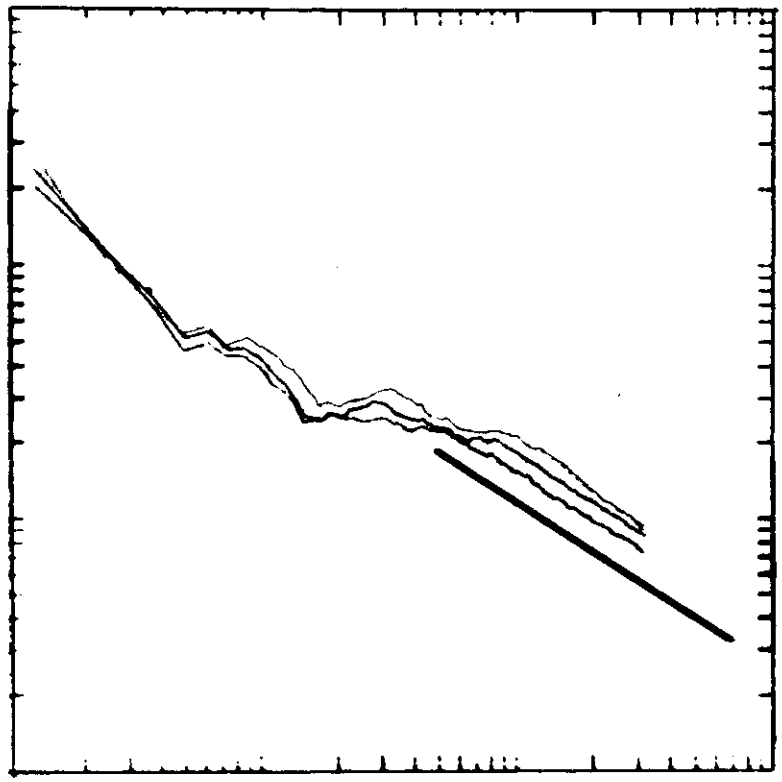

Fig. 4.6. Power spectra, fS(f) of the lateral velocity component v for each of the three sonic anemometers in operation during the BOREX 80 RUN 6 experiment. The sampling frequency is 25/4 Hz and the corresponding Nyquist frequency 25/8 Hz. The full-line drawn has a slope equal to -2/3.

lytical expressions of the form: $\rho = a + b \log_{10}(D)$. Such a relation applies strictly, of course, only to values of D between the shortest and the longest mast separation, which is 4.5 and 30 metres, respectively. In Fig. 4.7 the coefficients a and b have rather heuristically been estimated on the basis of the three separations available, and from here the cross-correlation coefficient for the lateral velocity components in Run 6 reads: $\rho_v = 1.05 - 0.20 \log_{10}(D)$.

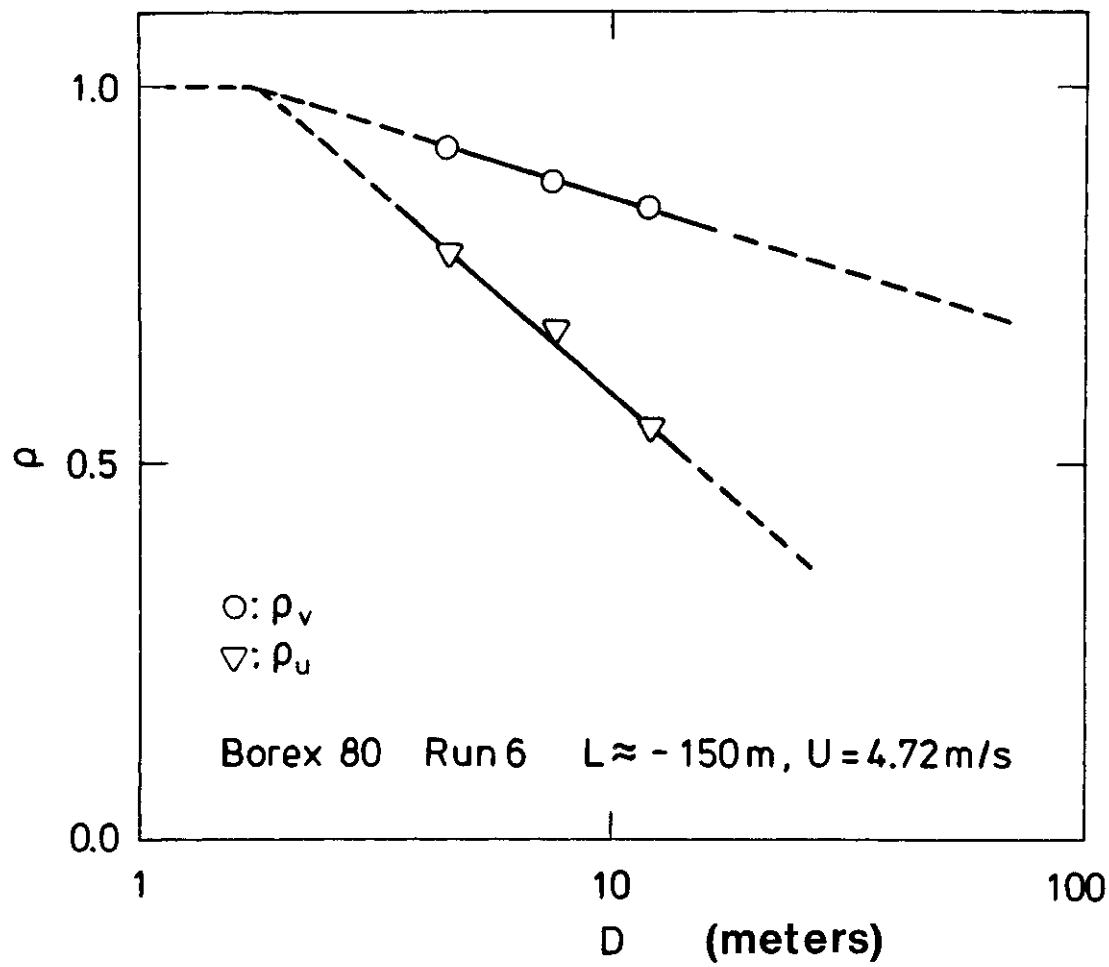

Fig. 4.7. Cross-correlation coefficients ρ of the two horizontal velocity components u and v measured during the BOREX 80 RUN 6 experiment, as function of the lateral displacement D.

The straight line fitted to the three measured values of the v cross correlation coefficient reads: $\rho_v = 1.05 - 0.20 \log_{10}(D)$, whereas the corresponding line for the u-correlation coefficient is $\rho_u = 1.14 - 0.54 \log_{10}(D)$.

4.3 The smoke release experiment, BOREX 81 run 1B

Because of the unforeseen troubles encountered with the data registration system and the sonic anemometer in mast 4 during the 1980 experiment, it was decided to extend the experimental campaign by another period during the summer 1981. The entire experiment was therefore reestablished at the site in the Borris Sönderland moors during the period from August 23 to 29, 1981.

A total of 10 runs were obtained in one week, and no severe troubles were encountered with the data registration system, or the sonic anemometers. During this experiment weather conditions were dominated by somewhat stronger winds, mostly coming from northerly and westerly directions, and the atmospheric stability was close to neutral during the day. Detailed data analyses of all 10 runs obtained has not yet ended, and a detailed report will be given here only on Run 1B, which was successful both with respect to the smoke and wind data registration.

In the morning of Monday the 24, clouds at approximately 3000 feet covered the sky at the experiment site, and the wind came rather strongly out of the W-NW direction at 5-8 m/s. The 2-m temperature was 15.0 ^{o}C and the relative humidity 40%. The atmospheric stability was judged to be close to neutral in agreement with the Monin-Obukhov length later obtained from the sonic anemometers.

At 11.30 a.m. the wind had turned in an almost perpendicular direction to the mast array and over the subsequent 40-min smoke release period the mean wind direction was found to differ by less than ~ 20 degrees from the predefined x-axis of the set-up. This time a series of 21 useful pictures was obtained from approximately 2000 feet above the release point. As a consequence of the stronger wind conditions during this experiment, the smoke plume was visible at downwind distances to 250-500 metres only.

Figures 4.8 and 4.9 show in a way similar to 4.4 and 4.5 the instantaneous standard deviations σ_r as well as the centroid dispersion $(\overline{y_{cm}^2})^{1/2}$ and single-particle dispersion Σ. In this experiment, a power law $\overline{\sigma_r} \propto x^{0.8}$ seems to fit the observations better than the linear relation suggested by Smith and Hay. The latter has been plotted with the intensity i = 0.28 calculated in Table 4.4. In this table the lateral intensity i_v has been calculated to ~0.20, and the corresponding absolute diffusion relation $\Sigma = i_v x$ has also been added to the data in Fig. 4.9. The Monin-Obukhov stability length measured by the sonic anemometer indicates a slightly unstable surface layer (cf. Table

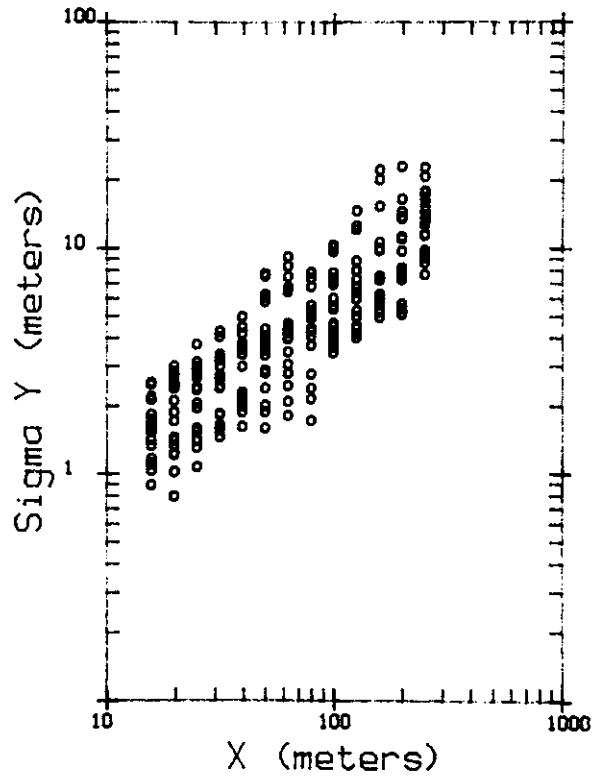

Fig. 4.8. Observed instantaneous standard deviations σ_r during the BOREX 81 RUN 1B experiment as a function of downwind distance x.

Table 4.4. Smoke release experiment: BOREX 81 RUN 1B

MAST No.	U	$\overline{u^2}$	$\overline{v^2}$	$\overline{w^2}$	$\overline{\theta^2}$	u_*	L
	m/s	$(m/s)^2$	$(m/s)^2$	$(m/s)^2$	K^2	m/s	m
1	5.88	1.03	1.43	0.359	0.099	0.447	-69
2	5.72	0.942	1.49	0.363	0.068	0.425	-98
3	5.93	0.974	1.39	0.361	-	0.443	
4	6.20	1.09	1.45	0.321	0.052	0.426	-99
MEAN	5.93	1.01	1.44	0.351	0.073	0.435	-90

$\theta = 20.9^{\circ}$ $\qquad z_i = 950$ m

$i_v = \sqrt{1.44}/5.93 = 0.202$

$i = (\sqrt{1.01 + 1.44 + 0.351})/5.93 = 0.280$ $\qquad w_* = 3.0u_*$

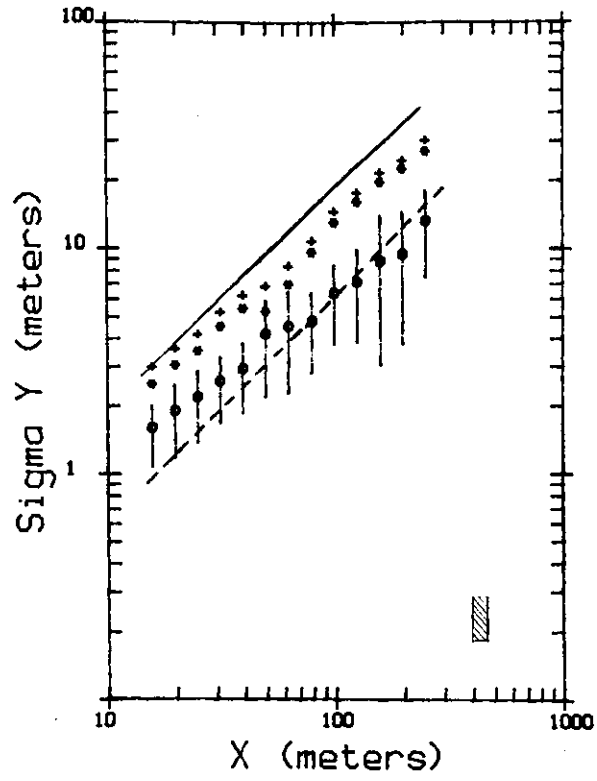

Fig. 4.9. Ensemble-averaged standard deviation $\overline{\sigma_r}$ of the instantaneous spreads shown in Fig. 4.8. As in Fig. 4.5, the cross-bars represent the standard deviation of the ensemble at a particular downwind distance. The centroid dispersion $(\overline{y_{cm}^2})^{1/2}$ is indicated by $\star$ and the total or single-particle dispersion by +.

The solid line, $\Sigma = i_v x$, represents the near-field limit of Taylor's (1921) (single particle) diffusion theory whereas the stipled line is Smith and Hay's (1961) formula: $\overline{\sigma_r} = 0.22\ ix$ for the expansion of a three-dimensional isotropic Gaussian puff.

As in Fig. 4.5, the shaded vertical bar represents the statistical uncertainty (+/- one standard deviation) of $\overline{\sigma_r}$.

4.4). The data obtained from the radio-sonde launched at 11.00 a.m. (see Fig. 4.10) also shows a decrease in potential temperature θ close to the ground. Above $z \approx 50$ metres the virtual temperature follows a neutral lapse rate up to the inversion height, which is approximately ~950 m in Fig. 4.10.

The measured cross correlation coefficients ρ are represented in Fig. 4.11 for all three velocity components and for the six

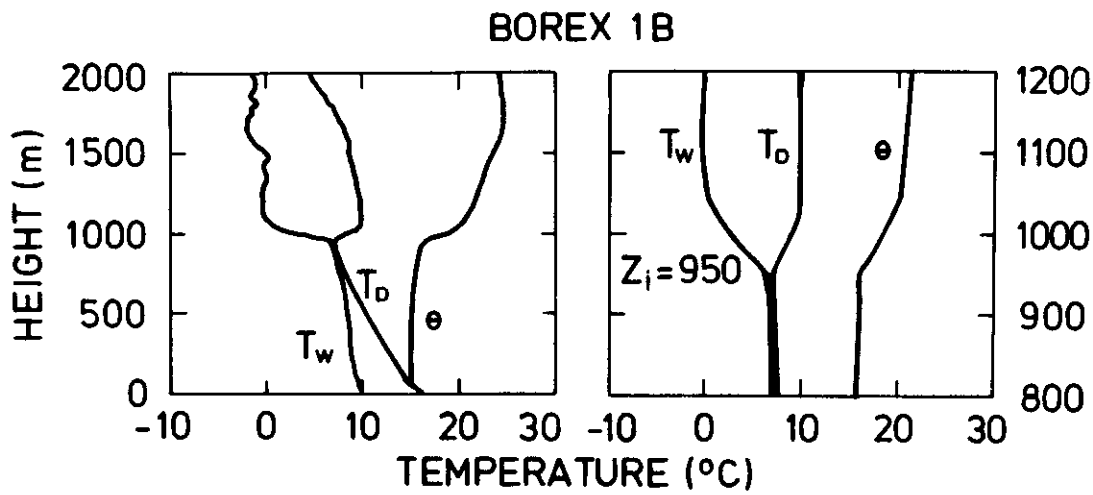

Fig. 4.10.

a) Radiosonding at 11.00 a.m. during the BOREX 81 RUN 1B experiment.
T_w: wet bulb temperature as function of height z
T_D: dry bulb temperature as function of height z
θ : virtual temperature as function of height z

b) As a) but with the vertical axis expanded between 800 and 1200 metres. The atmosphere is seen to be saturated immediately below the inversion height $z_i \approx 950$ m.

different lateral displacements possible in the BOREX 81 Run 1B experiment. Due to the inclination of the mean wind with the x-axis of the order 20° during this run, the six lateral displacements have been corrected by the factor cos(20°) and the maximum lateral displacement in Fig. 4.11 is therefore only 28 metres in contrast to the 30 metres in BOREX 80 Run 6. An empirical fit to the lateral correlation coefficient is $\rho_v = 1.07-0.285 \log_{10}(D)$. This expression is representative only for displacements D between 3 and 30 metres. The correlations in Fig. 4.11 are found to decrease with distance D faster than the corresponding correlation coefficients in the more unstable Run 6 in Fig. 4.7. Again, this agrees with the previously given explanation that in the case of an unstable boundary layer, where larger and thereby more coherent eddies are present which are then responsible for a bigger spatial correlation in the turbulence.

Finally, for BOREX 81 Run 1B, Fig. 4.12 a-c shows the power spectra obtained with the program FFT/COHERENCE. The Nyquist fre-

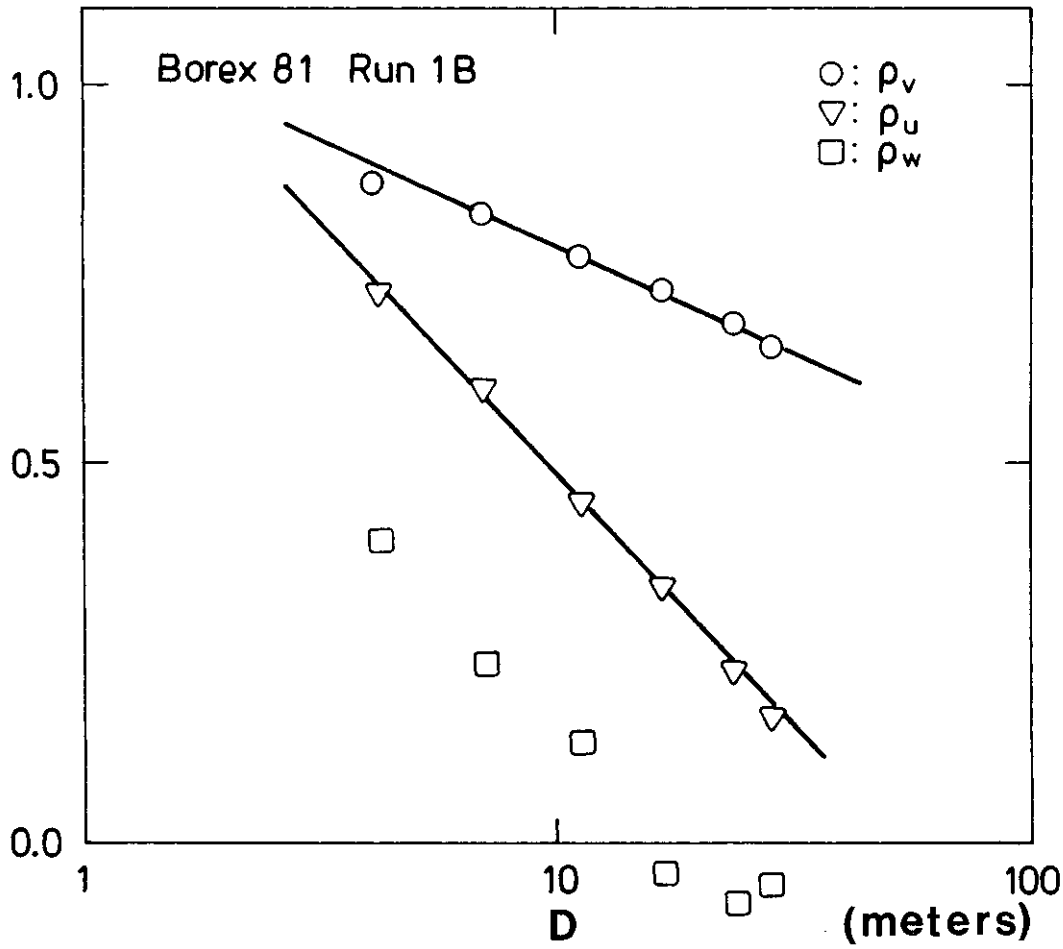

Fig. 4.11. Cross-correlation cooefficients ρ for each of the three velocity components u, v, and w measured during the experiment BOREX 81 RUN 1B, as function of the lateral displacement D. The line fitted to the six measurements of the lateral (v) correlation coefficients reads: $\rho_v = 1.07 - 0.285 \log_{10}(D)$, and the corrresponding line for the u-correlation coefficient is $\rho_u = 1.15 - 0.66 \log_{10}(D)$.

quency is here again 10 Hz. The horizontal spectra are in accordance with observations and models for velocity spectra in an unstable boundary layer (see, for instance, Højstrup, 1982). A peak in the vertical spectra is found at $f_p \approx 0.2$ Hz which corresponds to a dimensionless peak frequency $n_p = f_p z/\bar{u}$ equal to ~ 0.4. This value is characteristic of a vertical spectrum in a slightly unstable boundary layer (see, for instance, Busch, 1973).

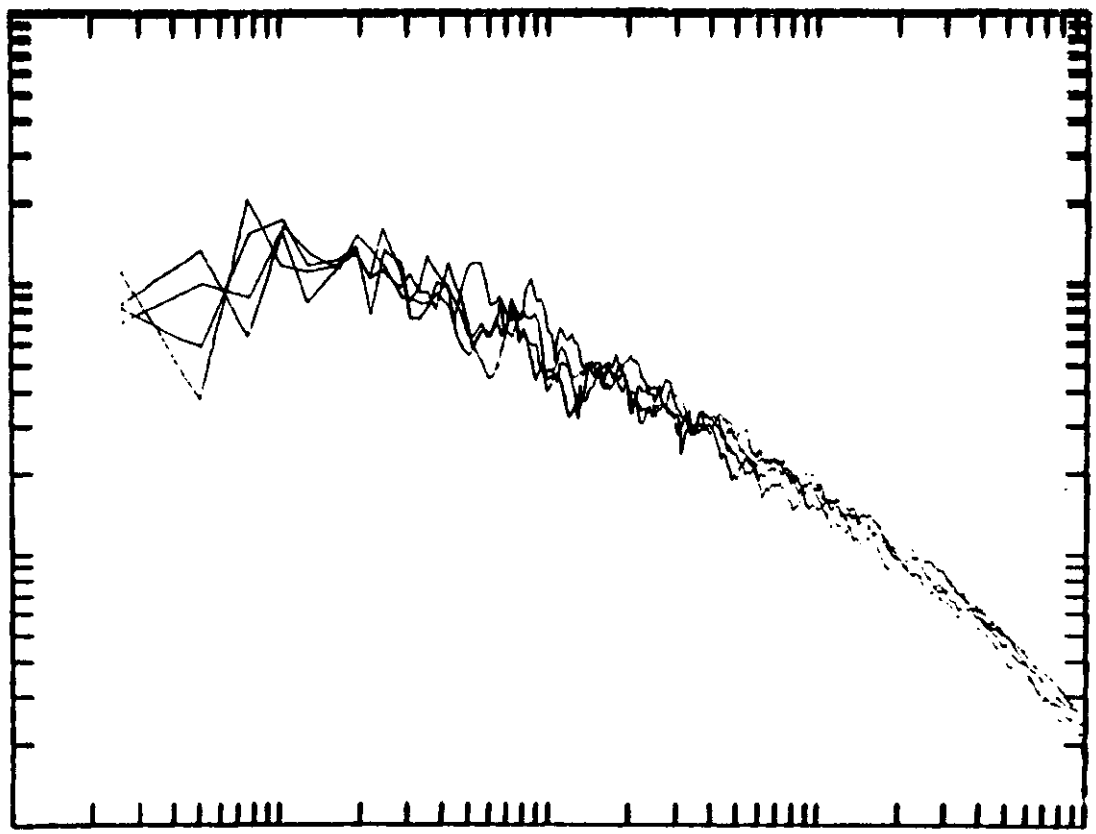

Fig. 4.12a. Power spectra as a function of wavenumber kS(k), of the four u-components obtained from the sonic anemometers in the smoke release experiment BOREX 81 RUN 1B. These spectra are calculated with the program FFT/COHERENCE (see Fig. 3.1b).

Plot of spectrum:	BOREX/FFT/RUN 1B: u-components
Spectrum multiplied by:	k
Mean wind speed U:	5.93 m/s
Number of raw estimates:	4096
Sampling period:	0.050 secs
Relative bandwidth:	0.20
Range of k:	10^{-3},10
Range of ordinate:	10^{-3}, 1

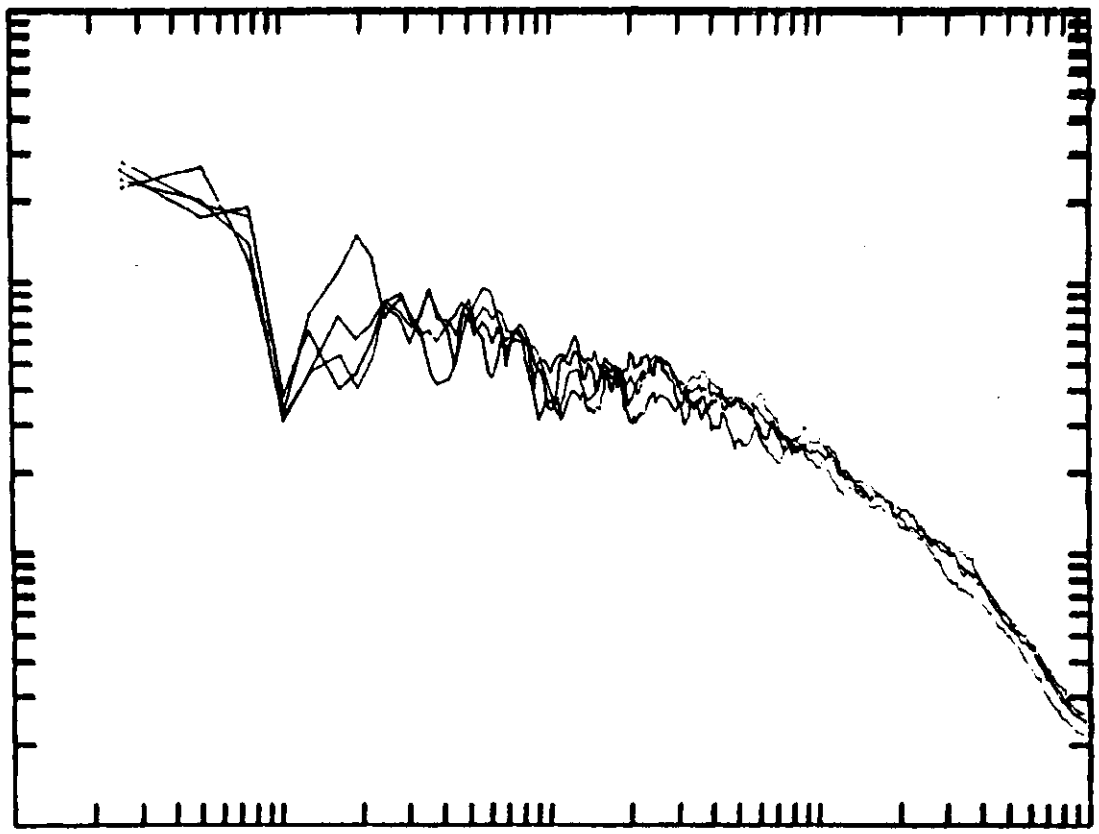

Fig. 4.12b. As Fig. 4.12a, but for the four v-components

Plot of spectrum:	BOREX/FFT/RUN 1B: v-components
Spectrum multiplied by:	k
Mean wind speed U:	5.93 m/s
Number of raw estimates:	4096
Sampling period:	0.050 secs
Relative bandwidth:	0.20
Range of k:	10^{-3},10
Range of ordinate:	10^{-3},1

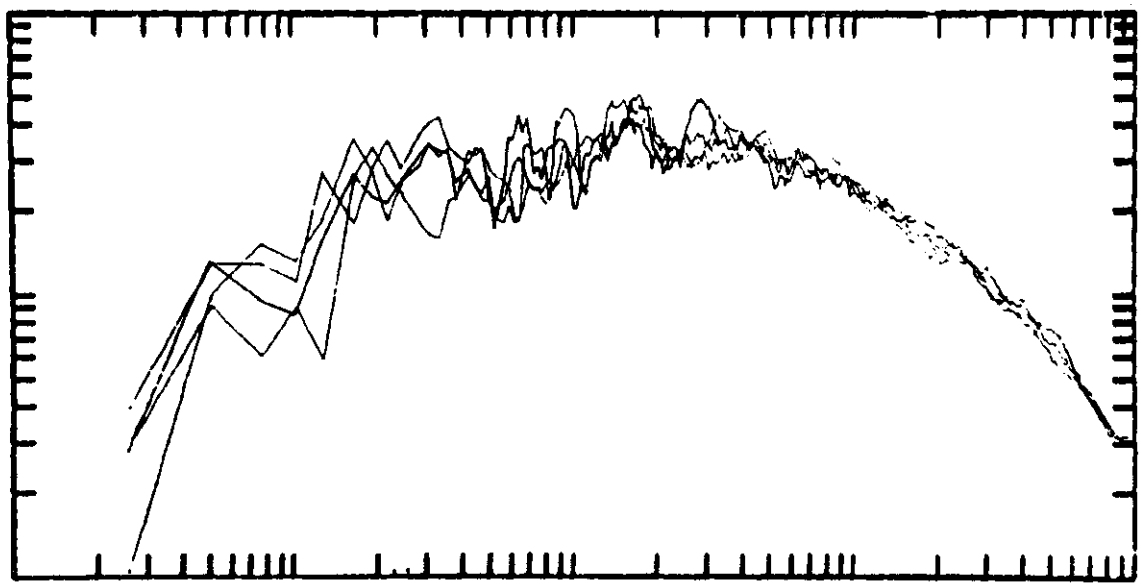

Fig. 4.12c. As Fig. 4.12a, but for the four w-components.

Plot of spectrum:	BOREX/FFT/RUN 1B: w-components
Spectrum multiplied by:	k
Mean wind speed U:	5.93 m/s
Number of raw estimates:	4096
Sampling period:	0.050 secs
Relative bandwidth:	0.20
Range of k:	10^{-3}, 10
Range of ordinate:	10^{-3}, 10^{-1}

5. EVALUATION STUDY OF RELATIVE DIFFUSION THEORY AND PUFF MODEL PERFORMANCE

5.1 Comparison of the instantaneous plume dispersion with the statistical theory on the turbulent diffusion of Gaussian puffs

The statistical theory (Mikkelsen, 1982c) of the turbulent diffusion of Gaussian puffs will be investigated by a comparison of the instantaneous smoke plume dispersion as observed during the BOREX 80 RUN 6 and the BOREX 81 RUN 1B field experiments. Let σ_p denote the lateral standard deviation (in the y-direction in Fig. 2.2) of a Gaussian cloud or puff released at the source point x = 0 at time t = 0. The situation is described by the

statistical theory which in the present notation yields the following set of equations for determining $\sigma_p(t)$ (cf. Mikkelsen, 1982c, Eqs. (3.37) and (3.38)).

$$\frac{1}{2}\frac{d\sigma_p^2}{dt} = \overline{v_p^2}(t)\cdot t_p(t) \tag{5.1}$$

where the velocity scale appropriate for the relative diffusion process in Eq. (5.1) is

$$\overline{v_p^2}(t) = \overline{v^2}\left\{1 - \int_{-\infty}^{\infty} \rho_v(\xi)\,\frac{1}{2\sqrt{\pi}\sigma_p(t)}\exp\left(-1/4\,\frac{\xi^2}{\sigma_p^2(t)}\right)d\xi\right\} \tag{5.2}$$

The time scale appropriate for the relative diffusion process, $t_p(t)$, is also given by Mikkelsen (1982c), Eq. (3.39). However, in the small time limit considered here, the puff travel time t can be assumed to be small relative to the Lagrangian integral time scale of turbulence, t_L. In this case it can be shown that $t_p(t) \simeq t$ (cf. Mikkelsen, 1982c, Eqs. (3.63) and (3.64)). A simple model for t_p, which is consistent with the near-field limit $t_p(t) \simeq t$ and which in addition provides a simple first-order correction when t becomes of a magnitude comparable to t_L, has also been included in the present investigation

$$t_p(t) = \frac{t_L}{1+t_L/t}\,, \tag{5.3}$$

(see also Mikkelsen, 1982c, Eq. (4.11)). By specifying the lateral velocity variance $\overline{v^2}$ and the cross-correlation function ρ_v in accordance with the quantities obtained during the experiments, the set of equations (5.1) to (5.3) has been solved numerically for σ_p as a function of the diffusion time t, and by use of the relation $x = \bar{u}t$, the predicted puff size σ_p could be compared with the observations of the ensemble mean value of the instantaneous plume width, $\overline{\sigma_r}$, as a function of downwind distance.

Figure 5.1 shows the numerical solution for $\sigma_p(x)$ obtained from Eqs. (5.1) and (5.2) with the variance and lateral cross-corre-

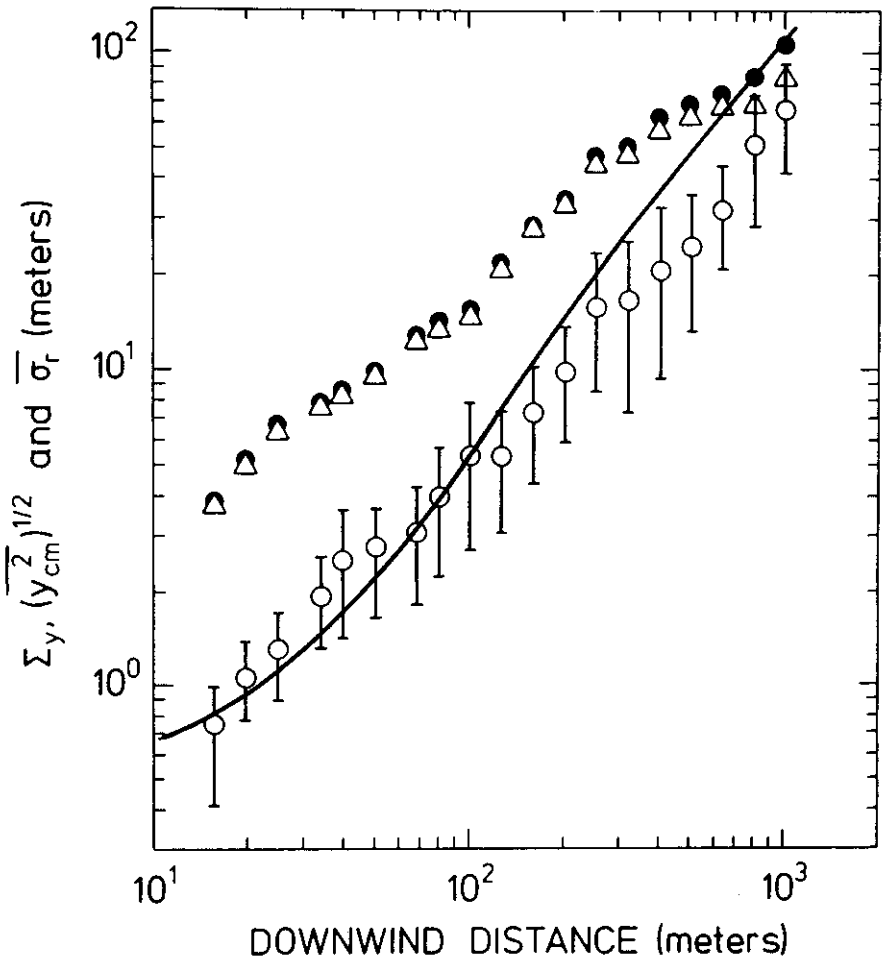

Fig. 5.1. Numerical solution of $\sigma_p(x)$ obtained from the statistical diffusion theory Eq. (5.1) - Eq. (5.3). The curve is shown on the instantaneous smoke data observations obtained from the BOREX 80 RUN 6 experiment. $\overline{u^2}$ = 0.62 m^2/s, $\sigma_p(0)$ = 0.5 m; $t_L = \infty$. $\rho_v = 1.05 - 0.20\log_{10}(D)$

lation coefficient ρ_v measured during the experiment BOREX 80 RUN 6. The initial puff size $\sigma_p(0)$ has been set equal to 0.5 metres and the time scale t_L is assumed to be large compared with the diffusion times t involved, that is, $t << t_L$ has been assumed here. Since the measured correlation coeficient ρ_v = $1.05 - 0.20 \log_{10}(D)$ applies only for values of the separation $D > D_o \simeq 2.5$ metres, say, it has been necessary to consider the contribution from the integral in Eq. (5.2) for values of $|\xi| \leq D_o$ as an undetermined constant. In Fig. 5.1 and in the later calculations of $\sigma_p(t)$ as well, the value of the part of the integral for which $|\xi| \leq D_o$ has consequently been chosen in order to give best agreement between the theory and the observa-

tions at the shortest distances considered. At longer distances, where the cloud had become large relative to D_o, the solutions for $\sigma_p(x)$ were found to be insensitive to the initial value chosen for this integral.

At distances beyond approximately 100 meters in Fig. 5.1 the calculated curve for σ_p is found to grow faster than the corresponding observations. Even though $\sigma_p(t)$ curves downward again beyond the distance of 200 metres, the theoretical prediction seems to be too high at $x \approx 500$ metres if the measurements at these far distances are taken into consideration.

Under all circumstances, a better overall agreement is obtained if the time scale model (Eq. (5.3)) is included. In Fig. 5.2,

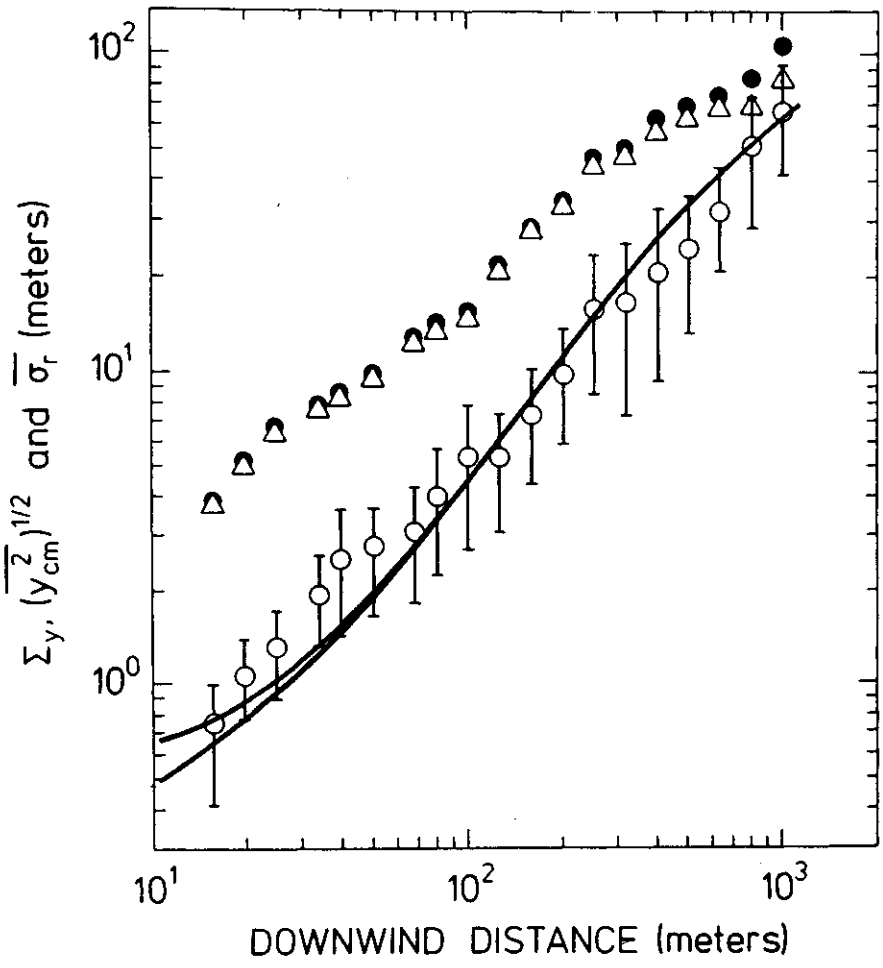

Fig. 5.2. As Fig. 5.1 but with t_L = 100 s and for two different initial values: $\sigma_p(0)$ = 0.5 metre (upper curve) and $\sigma_p(0)$ = 0.25 metre (lower curve).

the time scale t_L has been set equal to 100 sec. In addition, two different initial puff sizes, $\sigma(0) = 0.5$ and $\sigma(0) = 0.25$, have been used here. Even though the theoretical predictions now fall inside the vertical confidence intervals in Fig. 5.2, the calculated curve for σ_p exhibits an s-shaped form, whereas the observations rather seem to indicate a power law relationship between spread and downwind distance. We shall revert to this point when a similar comparison between the theory and observations from BOREX 81 RUN 1B has been performed.

Figure 5.3 is included in order to illustrate that the observed spatial cross-correlation coefficient ρ_v <u>is</u> in fact an important quantity for the calculation of the cloud growth rate in a given

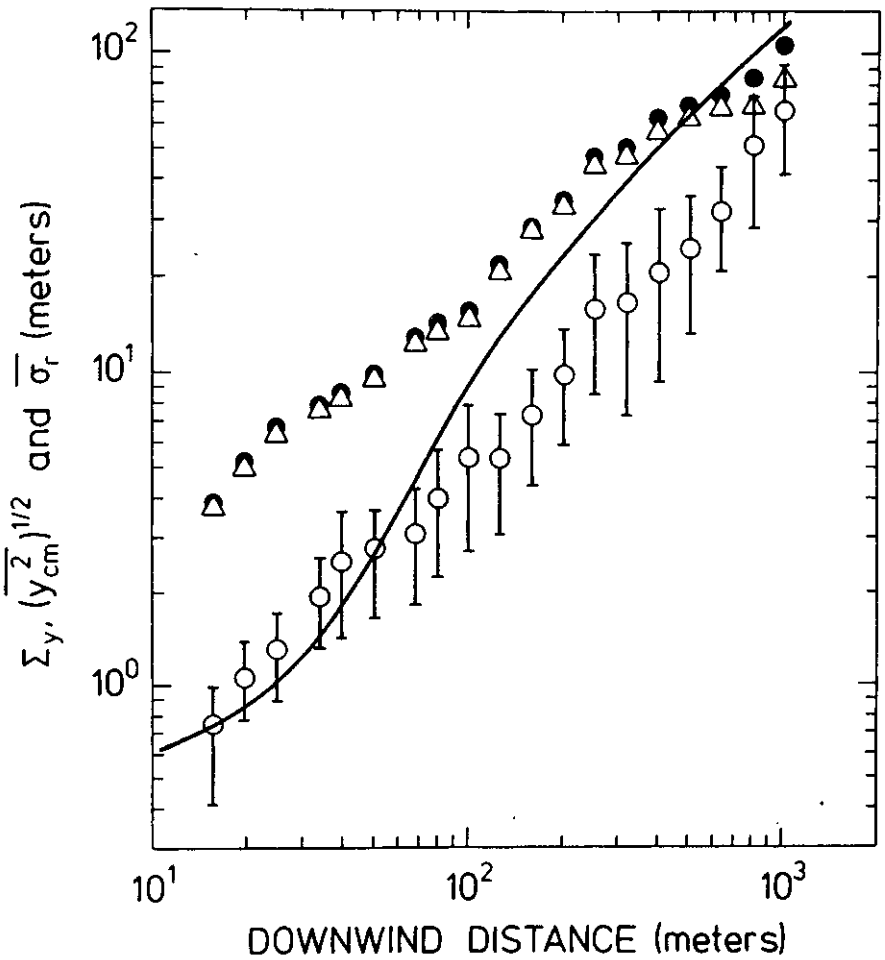

Fig. 5.3. As Fig. 5.1 but calculated on the basis of the u-correlation coefficient $\rho_u = 1.14 - 0.54 \log_{10}(D)$. $\overline{u^2} = 0.62$ m^2/s, $\sigma_p(0) = 0.5$ m, $t_L = 100$ s.

experiment. The figure shows a calculation of $\sigma_p(t)$ with t_L = 100 secs and otherwise initialized as in Fig. 5.2. But instead of ρ_v, ρ_u is used from the same experiment. The cross correlation coefficient ρ_u falls off with separation much faster than the corresponding ρ_v coefficient, and consequently the predicted spread is found to be far too big already after 100 metres downwind travel distance.

Figure 5.4 shows the calculated curve of $\sigma_p(t)$ from the more neutral stratified experiment BOREX 81 RUN 1B. Here, ρ_v = $1.07 - 0.285 \log_{10}(D)$ for $D \geq 3.5$ metres, $\overline{v^2} = 1.44$ m^2/s^2 and t_L is set equal to 100 sec as before. The initial size $\sigma_p(0)$ is set equal to 1 metre. The prediction falls inside the scatter in the observations, and there is also a tendency of an "s-shaped" prediction curve. The observations, on the other hand, rather seem to obey a linear relation in the log-log plot shown.

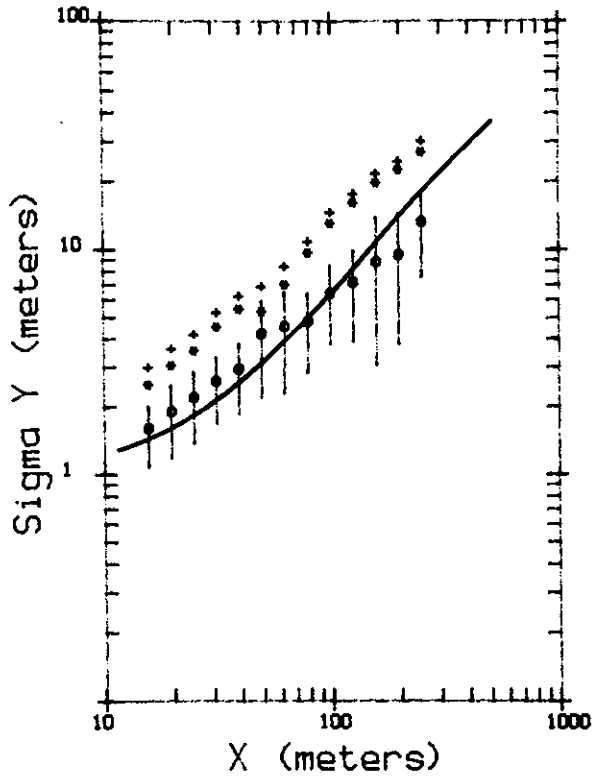

Fig. 5.4. Numerical solution of the instantaneous cloud diffusion $\sigma_p(x)$ shown together with the instantaneous smoke data observations from the BOREX 81 RUN 1B experiment. $\overline{v^2} = 1.44$ m^2/s^2, $\sigma_p(0) = 1.0$ m; $t_L = 100$ s. $\rho_v = 1.07 - 0.285 \log_{10}(D)$.

A possible explanation for the difference between the shape of the calculated curve $\sigma_p(x)$ and the observations $\overline{\sigma_r}(x)$ will now be suggested.

The spread $\sigma_p(x)$ calculated from the model, Eq. (5.1) - Eq. (5.3), is based on the measurements of the turbulence from the mast array at 10 meters height. The smoke plume, on the other hand, starts its expansion in the turbulence close to the ground, at heights of the order of one meter. The total variance $\overline{v^2}$ can be assumed to be approximately constant throughout the surface layer in which the observations of the visible smoke took place. However, the peak frequency f_p in the energy spectrum of the lateral spectrum $S_v(f)$, corresponding to the lateral correlation coefficient $\rho_v(D)$, will be shifted towards lower frequencies as a function of the height of observation z, approximately as $f_p = n_p\bar{u}/z$ (Busch, 1973). That means that a small cloud released close to the ground initially will experience a relatively higher level of turbulent kinetic energy in the high-frequency end of the spectrum than the mast array measures at the 10-m level.

Since the high frequency end of the turbulence is very efficient for the inital spreading, the smoke cloud can be expected to grow faster than the model prediction in the beginning when the mean cloud height is smaller than the measuring height. On the other hand, when the mean height of the cloud has increased to a size which is larger than the measuring height, the spectral energy levels measured at the top of the mast are expected to be higher than the corresponding energy levels experienced by the smoke cloud. The predicted curve for σ_p can therefore be expected to overestimate in this case. Consideration of the results in Figs. 5.2 and 5.4 shows that the intersection of the calculated and observed spreads actually takes place when the cloud is of a size comparable with the measurement height z = 10 metres. (It has been assumed here that the vertical cloud size also is a measure of the horizontal size.)

In summary, it can be claimed that the simple relative diffusion model Eqs. (5.1) to (5.3) shows promise for predicting the over-

all behaviour of the observed instantaneous smoke diffusion during the experiments BOREX 80 RUN 6 and BOREX 81 RUN 1B. However, due to the vertical inhomogeneity caused by the presence of the ground, the smoke observations and the relative diffusion model are not directly comparable.

5.2 Comparison of the smoke plume observations with computer simulations using the small-scale Risø Puff Diffusion Model

A qualitative intercomparison has been made between instantaneous smoke diffusion simulations based on the small scale puff diffusion model (Mikkelsen, 1978, and Mikkelsen, 1982a) and the visible smoke plume observations from the experiment BOREX RUN 6.

By use of a concurrently measured time series of the turbulent wind field as registered by the sonic anemometer closest to the source point, the puff model is able to simulate the instantaneous smoke plume by advecting a series of sequentially released puffs in a three-dimensional computational grid. In a horizontal plane the puffs are assumed to be Gaussian distributed whereas the puff's vertical distribution and growth depend on the atmospheric stability (see Mikkelsen, 1982b). All the puffs present in the grid are simultaneously advected by the windfield measured at the release point and their horizontal growth are calculated by the formula of Smith and Hay (1961) discussed earlier. For a more detailed description and documentation of the Risø puff model, the reader is referred to Mikkelsen (1979) and Mikkelsen (1982a and 1982b).

Fig. 5.5. A consecutive series of 14 instantaneous smoke plume contours (solid lines) obtained from the aerial photographs during the BOREX 80 RUN 6 experiment. The smoke plumes (black area) extend from the source point, over the contrast plates (dots) the outermost row of which is 500 meters downwind. The tic marks on the axes are spaced 50 meters apart. On top of each plume contour is shown the corresponding puff model simulation (circles) of the instantaneous smoke plume.

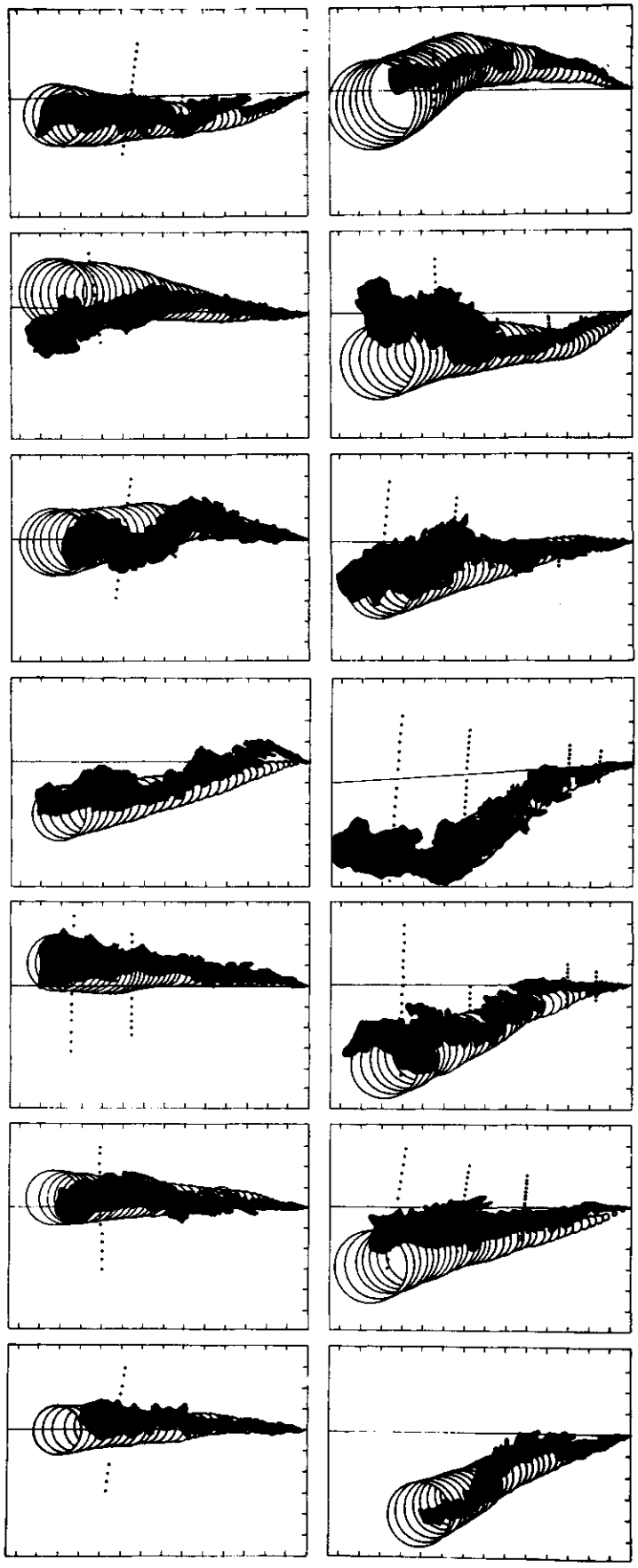

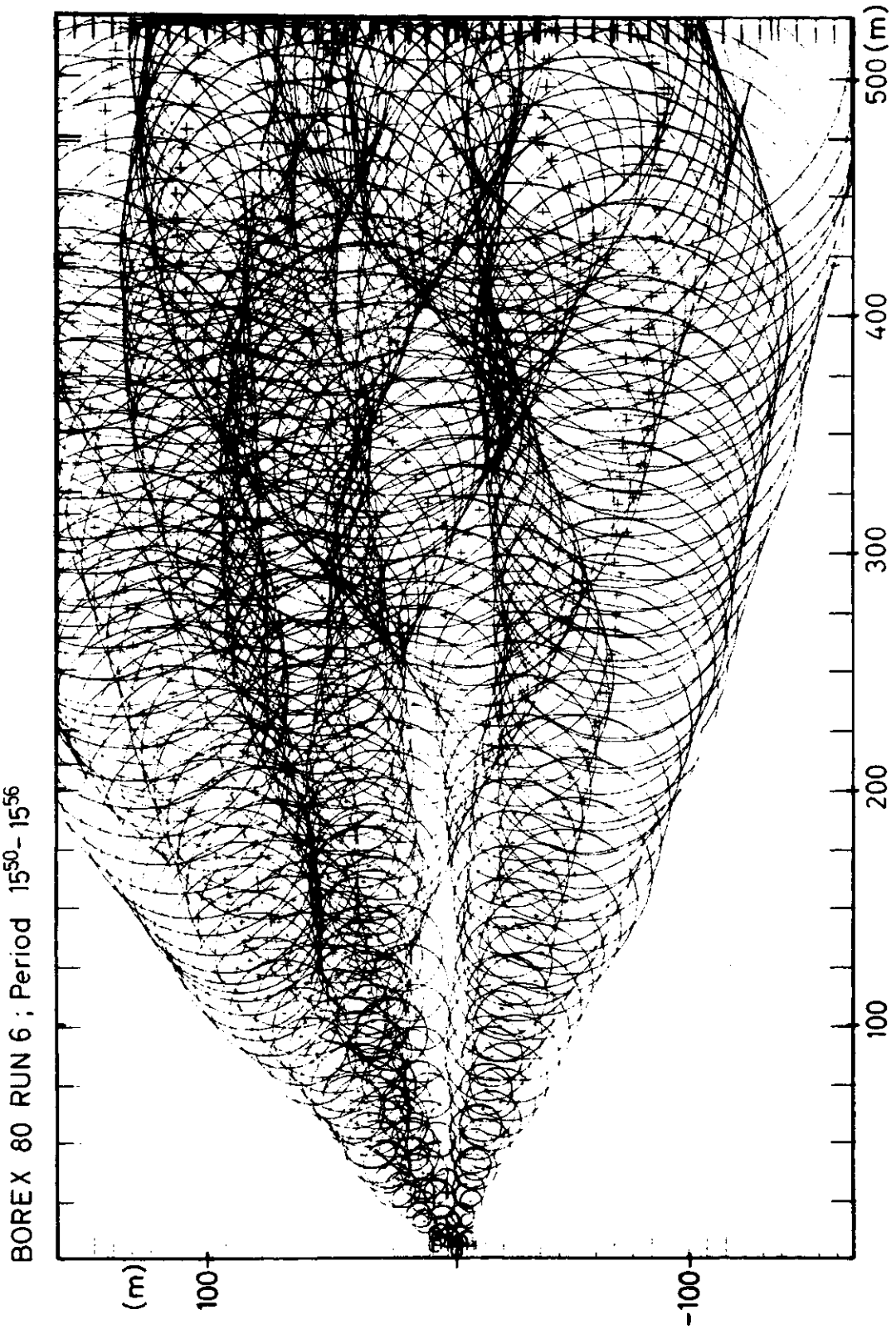

Fig. 5.6. Instantaneous smoke plume simulations calculated with the puff model for ten 30-sec consecutive intervals from the last 5 minutes of the BOREX 80 RUN 6 experiment. The simulation shows a strongly meandering plume extending from the source point and downwind to approximately 500 metres.

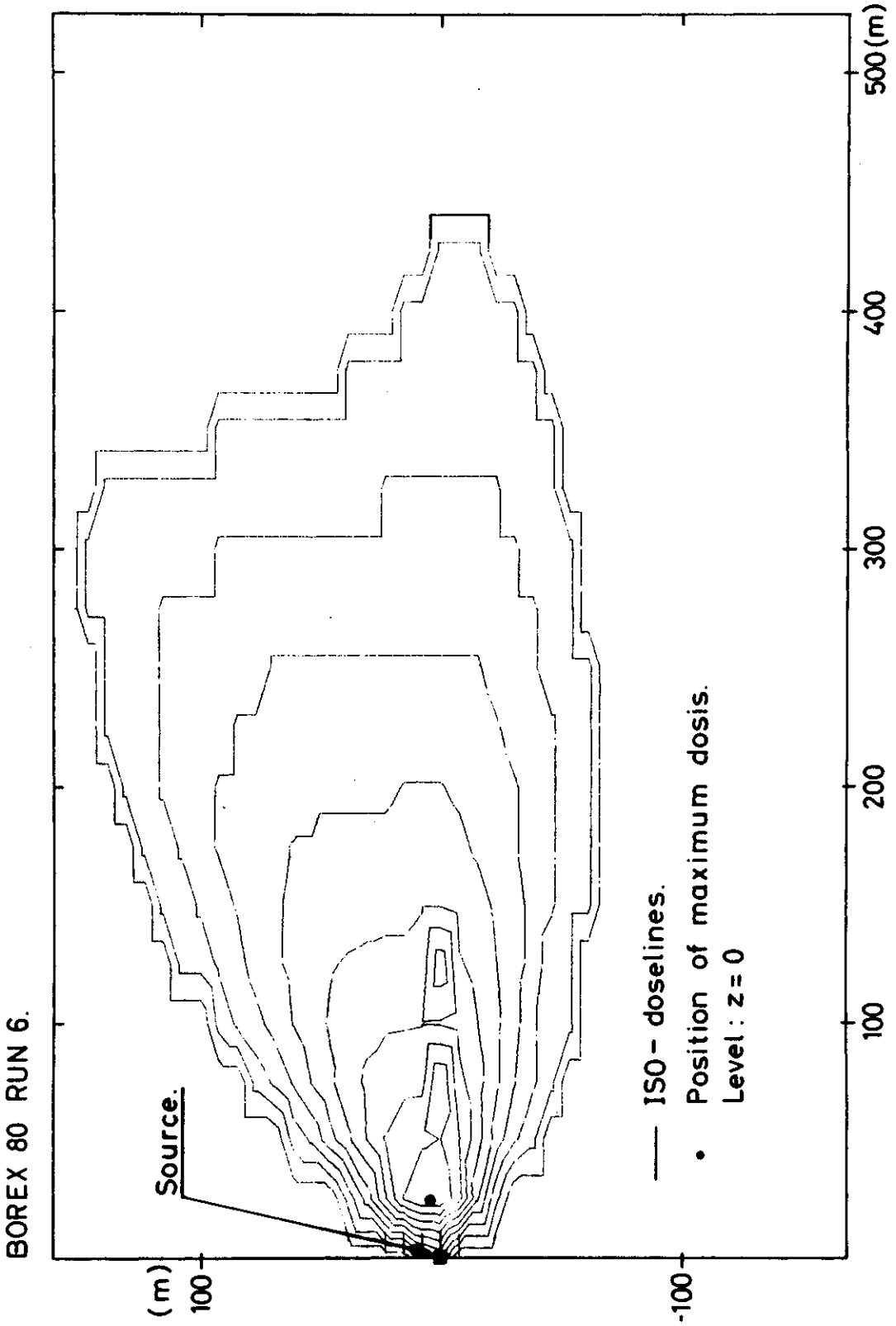

Fig. 5.7. Ground level time-integrated concentration doses calculated by the puff model corresponding to the BOREX 80 RUN 6 experiment from a total release time equal to 40 min. ISO-concentration dose lines are shown for maximum dose D_{max} $gsm^{-3}/2^n$; n = 1, 2, ...10. Assumed release rate: 1 g/s. D_{max} = 0.26 gsm^{-3}. Release height 1 metre.

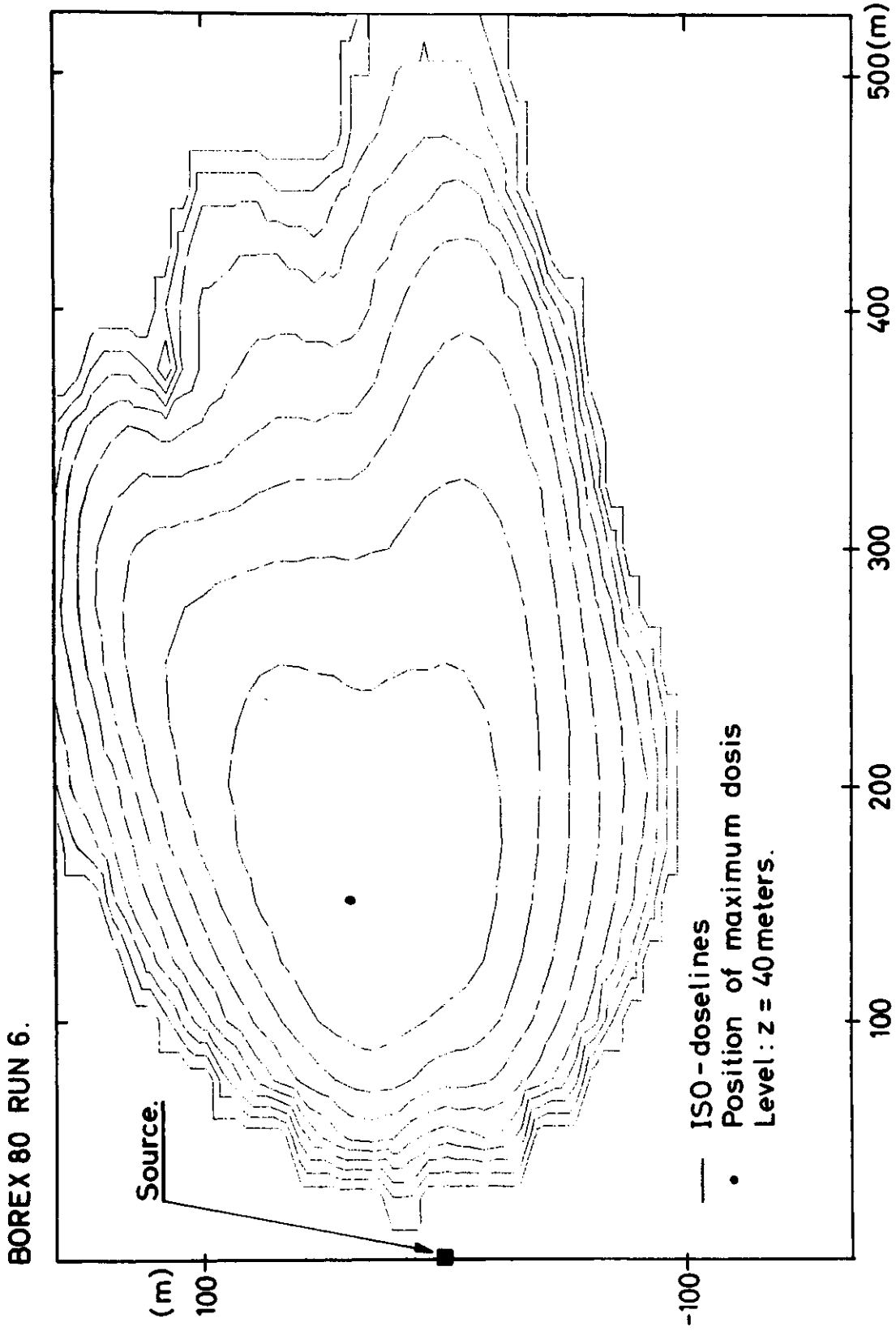

Fig. 5.8. As Fig. 5.7 but at z = 40 metres instead of at ground level. D_{max} = 0.0035 gsm^{-3}.

Figure 5.5 compares a series of 14 instantaneous smoke plume contours observed from the airplane during the BOREX 80 RUN 6 experiment with the corresponding puff model simulations of the instantaneous plume. A direct comparison between the smoke plume contour and the puff chains is not possible beyond the 500-m marker plates due to the distortion caused by the relatively low cruising height of the airplane in this experiment. It is found, however, that the puff advection scheme based on a point measurement close to the release point shows promise at the downwind distance considered (up to ~ 500 metres) and for the neutral/unstable atmosphere in question.

Picture No. 4 in the top row shows the effect of a strong horizontal wind shear. Close to the source point the puff chain, which is advected by the wind field at the 10-m level, shows an angle to the observed smoke plume; at this short downwind distance it still is close to the ground. After some 50 metres of travel, however, the smoke plume had grown in the vertical to a height comparable with the measuring height, and at downwind distances hereafter, the simulated and the observed smoke plume seem to travel along rather consistently.

Ten instantaneous puff plumes, obtained during a six-minute period towards the end of the 40-minute long BOREX 80 RUN 6 experiment, have been added on top of each other. This is shown in Fig. 5.6 which indicates a period with extremely unstable and non-stationary conditions. The case shows a non-stationary situation where the puff model has great advantages over an ordinary plume model. Finally, Figs. 5.7 and 5.8 show the total time-integrated concentration at the ground level and at the 40-m vertical level, respectively, also obtained with the puff diffusion model. Both of these dosis graphs exhibit significantly more detailed structure than could have been obtained with a simple Gaussian plume model.

Unfortunately, the budget of the experiment did not allow for SF_6 tracer releases and sampling techniques to be used from which a direct comparison of the time-integrated concentration profiles from the puff model and the experiment would have been possible.

To summarize, it can be claimed that within the uncertainty unavoidably encountered when dealing with the atmospheric turbulent diffusion processes, the experiments seem to validate the use of the puff advection scheme and the puff growth rate equation implemented in the Risø puff diffusion model operating over the relatively short downwind distances considered ($x < 1000$ metres).

6. CONCLUSION

Studies of continuous ground level released smoke diffusion have been carried out in the surface layer over homogenous terrain with the object of evaluating methods and principles to be used with an operational, small-scale puff diffusion model.

The applicability of a proposed advection scheme for puffs (Mikkelsen, 1978 and Mikkelsen, 1982a), which is based on a time series of the wind velocity obtained from a single point measurement close to the source point, has qualitatively been investigated. This has been done by comparing the visible contour of the instantaneous smoke plume with computer simulations obtained with the puff model. Over the relatively small scale considered ($x < 1$ km), the advection scheme was found in large to be capable of simulating the instantaneous horizontal outline of the plume. At very short distances from the release point, smaller differences could occur in connection with plume rise and strong vertical inhomogenities in the wind field. So far, the experimental investigations of the single-point-based advection scheme have been limited to neutral-unstable atmospheric conditions only, where its performance is probably better than that in a stable atmosphere due to the presence of relatively large and coherent structures in the convective horizontal turbulent field. Similar experiments carried out during more stable atmospheric stratifications are therefore desirable in order to evaluate also the model performance here.

More quantitative investigations have been carried out on the applicability of the proposed statistical theory of puff diffusion (Mikkelsen, 1982c). Spatial velocity correlations have been measured as a function of lateral displacements by means of an array of four 3-axis sonic anemometers, and based on these measurements the puff's standard deviation σ_p has been calculated from the statistical theory as a function of downwind distance, at present for two independent experiments.

Observations of the visible plume width from an airplane have then been used in connection with the opacity method to establish an ensemble-averaged estimate of instantaneous diffusion, also as a function of the downwind distance. When it is taken into consideration that the diffusion was influenced by vertical inhomogeneities of the surface layer turbulence, a reasonable agreement has been obtained between the observed and the calculated dispersion.

However, in each of the two experiments considered, it has been necessary to modify the extrapolated velocity covariances for values of the lateral displacements D smaller than the minimum mast separation (4.5 m).

By taking the relatively large uncertainty of the smoke data observation and processing into account, the much simpler formula originally proposed by Smith and Hay (1961) (and later calibrated against experiments by Pasquill (1974)), were also found to be capable of predicting most of the observed instantaneous diffusion satisfactorily well.

The experiments investigated during the BOREX campaign are all rather limited with respect to scale and with respect to the variation in the atmospheric stability. It would therefore be incorrect to postulate that the statistical theory proposed for puff diffusion has been experimentally verified in general, especially since it has been examined it its (Eulerian) near-field limit only.

On the other hand, no systematic discrepancies between the obserservations and theory on the scale and over the stabilities considered have been discovered. This "reversed conclusion" encourages the performance of future investigations on larger scales and including larger variability of the atmospheric stability than was encountered during the present BOREX campaign.

7. ACKNOWLEDGEMENTS

Many people from many different organizations, including laboratories and universities in many countries have actively participated in the BOREX campaigns. Without their help the experiments would never have been possible.

First of all, civ.ing. M. Caspersen and civ.ing. P.H. Rasmussen of the Danish Defence Research Establishment are acknowledged for their support of the project and for providing access to the ideal experiment site and the smoke pots.

Professor W.K. George, University of Buffalo, is gratefully appreciated for his active participation in the 1980 experimental campaign and for actively taking part in the development of the data analysis programs.

I acknowledge also the participation in the 1981 experimental campaign of Dr. D. Lenschow, National Center of Atmospheric Research, Boulder.

Mr. Richard Eckman, a one-year visiting graduate student from Penn State University, is acknowledged for his interesting thesis work which has been of help in the project.

Also there should be room for in-house acknowledgments as well: Gunnar Dalsgård, Finn Hansen, and Anker Bruun Andersen for their skilled technical assistance without which the experiment

never could have taken place. Arent Hansen for his skilled and safe, but not always comfortable, piloting activity. My thesis advisor, mag.scient Leif Kristensen shall in this connection be acknowledged for his patient instructing in the use of the Risø data registration system and for advising me in the successful operation of the sonic anemometers. Finally, I shall not forget to thank Birthe S. Jørgensen for her careful typing of this report.

8. REFERENCES

BUSCH, N.E. (1973). On the Mechanics of Atmospheric Turbulence. In: Workshop on Micrometeorology. Ed. by P.A. Haugen. (American Meteorological Society, Boston, Mass.) 1-66.

GIFFORD, F.A. (1980). Smoke as a Quantitative Atmospheric Diffusion Tracer, Atmos. Environ. 14, 1119-1121.

HØJSTRUP, J. (1982). Velocity spectra in the Unstable Planetary Boundary Layer. J. Atmos. Sci. 39, No. 10, 2239-2248.

MIKKELSEN, T. (1979). Simulation of obscuration smoke diffusion. Work done under contract to the Danish Defence Research Establishment/Risø, 73 pp. Available from: Meteorology Section, Physics Dept., Risø National Laboratory, DK-4000 Roskilde, Denmark.

MIKKELSEN, T., S.E. LARSEN and I. TROEN (1980). Use of a Puff Model to Calculate Dispersion from a Strongly Time Dependent Source. In: Seminar on Radioactive Releases and their Dispersion in the Atmosphere following a Hypothetical Reactor Accident, Proceeding. Held at Risø, 22-25 April, 1980 (Commission of the European Communities, Luxembourgh) Vol. 2, 575-614.

MIKKELSEN, T. (1982a). Description of the Risø Puff Diffusion Model. Risø-M-2361.43 pp.

*MIKKELSEN, T. (1982b). A Parametric Description of a Skewed Puff in the Diabatic Surface Layer. Risø-R-476. 32 pp.

*MIKKELSEN, T. (1982c). A Statistical Theory on the Turbulent Diffusion of Gaussian Puffs. Risø-R-475. 77 pp.

PASQUILL, F. (1974). Atmospheric Diffusion. 2nd Ed. (Wiley, New York) 429 pp.

SCHOTANUS, P., F.T.M. NIEUWSTADT and H.A.R. DE BRUIN (1983). Temperature Measurements with a Sonic Anemometer and its Application to Heat and Moisture Fluxes. Boundary-Layer Meteorol. 26, 81-94.

---

*)These reports constitute together with the present report the thesis "FORMULATION AND EXPERIMENTAL EVALUATION OF AN OPERATIONAL PUFF DIFFUSIONn MODEL", cf. preface.

SMITH, F.B., and J.S. HAY (1961). The Expansion of Clusters of Particles in the Atmosphere, Q. J. R. Meteorol. Soc., 87, 82-101.

TAYLOR, G.I. (1921). Diffusion by Continuous Movements, Proc. Lond. Math. Soc. A. 20, 196-202.